High-Performance Adaptive Pressure Control in the Presence of Time Delays

PRESSURE CONTROL FOR USE IN VARIABLE-THRUST ROCKET DEVELOPMENT

ANIL ALAN, YILDIRAY YILDIZ, and UMIT POYRAZ

Digital Object Identifier 10.1109/MCS.2018.2851009
Date of publication: 18 September 2018

1066-033X/18©2018IEEE

Summary

The focus of this article is the pressure-control problem of gas generators employed in variable-speed rockets. The ability to change the speed during operation enables these rockets to adjust to the demands of different types of maneuvers and varying flight conditions. As a result, speed-controllable rockets provide a dramatic advantage over their alternatives with fixed speed profiles. In throttleable ducted rockets, speed variation is achieved by changing the fuel flow rate (throttleability), which requires a careful controller design. The article provides a detailed review of the current state of rocket propulsion control and the main challenges in the field. A controller (which contains a unique combination of traits such as fast adaptation, delay compensation, and provision of a smooth response) is introduced as a solution to the pressure control problem in air-breathing rocket propulsion. The superior performance of the controller, compared to existing alternatives, is demonstrated through experimental tests, using a test setup provided by Roketsan, Inc.

Smart defense systems using missiles that can fine-tune their velocity profiles have significant technological superiority over their conventional counterparts. This tuning is possible, in part, due to the deployment of advanced sensing, actuation, and computation capabilities and sophisticated guidance, navigation, and control algorithms. The capability to alter velocity during operation helps sustain optimum performance for different flight conditions. In addition, it makes it possible to slow down while turning and then speed up along a straight path, rendering the maneuvers more efficient. This ability to modify velocity (known as throttleability) is also known to increase a missile's no-escape zone, which is the maximum range that the missile can outrun its target [1]. As presented in "Summary," this article discusses the advanced control technologies needed to obtain throttleability.

To achieve throttleability, it is important to understand the underlying dynamics leading to jet-engine propulsion. Propulsion systems in jet engines generate thrust via a burning process that creates a chemical reaction between fuel and an oxidizer. These systems can be divided into two groups in terms of the source of the oxidizer: air-breathing jet engines (which get the oxidizer from the surrounding atmosphere) and non-air-breathing jet engines (which carry the oxidizer along with the fuel, making them closed systems). Conventional solid-rocket engines, which carry their fuel and oxidizer in a solid state, are examples of non-air-breathing jet engines. They are relatively easy to manufacture (since they do not contain complex moving parts) and produce standard thrust performance over a variety of flight conditions (since they are closed to their environments). Besides the advantage of simplicity, the thrust can also be controlled, which makes them variable-thrust solid propulsion systems [2]. However, the specific impulse values (the total impulse that a rocket engine can produce per unit of propellant burnt) is very low compared to air-breathing engine systems since it must also carry the oxidizers. As such, conventional solid-rocket engines are less preferable for long-range cruise flights. Air-breathing jet engines, on the other hand, compress the air during operation using various methods (such as ramjets, scramjets, turbojets, and turbofans) and mix it with the fuel for the combustion and to yield thrust.

THROTTLEABLE DUCTED ROCKETS

A ramjet is an air-breathing jet engine that utilizes forward motion to collect and compress air using air-intake openings. Ducted rockets are ramjet-type engines (see Figure 1). The air then moves to the ram combustor, where it is mixed with the oxidizer-deficient gaseous fuel provided by the gas generator (GG).

The GG uses a preburn process to produce the gaseous fuel from the solid propellant. The fuel is then sent to the ram combustor through a connection between the GG and the ram combustor by a pressure gradient. The appeal of the ducted rockets is the possibility to control the fuel flow rate (supplied by the GG) into the ram combustor, which transforms these rockets into throttleable ducted rockets (TDR). TDRs, therefore, combine the advantages of different propulsion systems: high specific impulse values of air-breathing engines; simplicity of solid rocket engines; and throttleability, which is available in liquid fuel ramjet engines, for example. Although the specific impulse values in TDRs are high, metallic particles (boron or aluminum) are typically placed inside the solid propellant to further enhance it [3], [4]. These particles are not burnt during the initial burning process at the GG and sent to the ram combustor with the gaseous fuel.

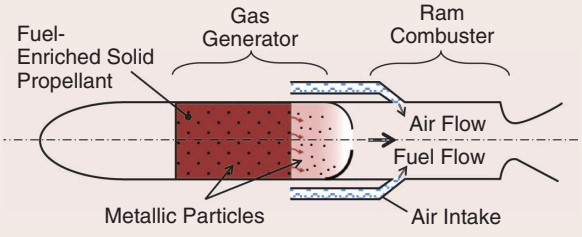

FIGURE 1 Throttleable ducted rocket (TDR) components. TDR propulsion systems contain two main parts, the gas generator (GG) and the ram combuster (RC). Fuel-rich (or oxidizer-deficient) solid propellant in the GG is ignited and partially burned to obtain fuel in the gaseous form, which is then sent to the RC to combine with air received and compressed by the air intakes for further combustion to produce thrust.

Alternative Methods of Obtaining the Variable Fuel Flow Rate

In TDRs, the flow rate of the gaseous fuel that is generated determines the amount of thrust. Various methods are used to obtain a variable fuel rate [5], [6], which are listed below and depicted in Figure 2.

- *Changing the burning area of the propellant in the GG in a controlled manner*: Assuming that the solid propellant burns within a uniform cross-sectional area (known as "cigarette-type burning"), such as in Figure 2(a), their solid grains can be trimmed to have different cross-sectional areas at each moment of burn. A smaller burning area generates less fuel and, therefore, less thrust. However, once a trimmed propellant is ignited, it is impossible to make any changes to its geometric structure during operation. Therefore, solid rocket engines with trimmed propellants have prescribed thrust profiles over all operating regions.
- *Introducing secondary injection to the GG chamber to control the burning rate*: It is known that the burning rate of a solid propellant is affected by the pressure of the chamber, where the relationship is determined by the pressure sensitivity of the propellant [7]. Therefore, the burning rate of the solid propellant can be controlled by controlling the pressure at the GG chamber. One way to achieve this is by introducing a secondary medium. However, this method requires complex parts, such as a secondary chamber.
- *Utilizing a vortex valve that introduces a swirl to the flow to control the effective throat area*: The injected fuel flow rate from the GG to the ram combustor depends on the effective throat area between the two parts. Therefore, changing the effective throat area can be counted as a method for manipulating the fuel flow rate. A vortex valve can induce a swirling flow at the throat to increase the flow resistance (or reduce the effective throat area) at the expense of increasing the system complexity.
- *Changing the throat area between the GG and the ram combustor using a control valve*: The effective throat area can be varied using a control valve, which is less complex than the vortex valve. Among the listed methods here, this method is used the most often ([5], [8]–[11]), and the control approaches discussed in this article assume the control valve is the actuator.

Control Solutions to Obtain Variable Speed or Thrust

There are two control solutions for the speed or thrust control problem of TDRs. The first solution forms a single-loop controller structure, where the controller calculates the necessary throat area between the GG and the ram combustor to track a given speed or thrust reference [8]–[12]. The block diagram for this solution is provided in Figure 3(a). The second solution creates a hierarchical control structure, where an outer-loop speed/thrust controller calculates the required GG pressure to obtain a desired speed or thrust profile, which is then used as a reference for the inner pressure control loohp, as shown in Figure 3(b), [1], [13]–[15].

These two control solutions have distinct advantages over each other. The single-loop solution is simpler to design. However, the hierarchical control structure is safer, due to gas pressure stability; it is easier to keep the pressure inside the GG within safe limits by utilizing a separate

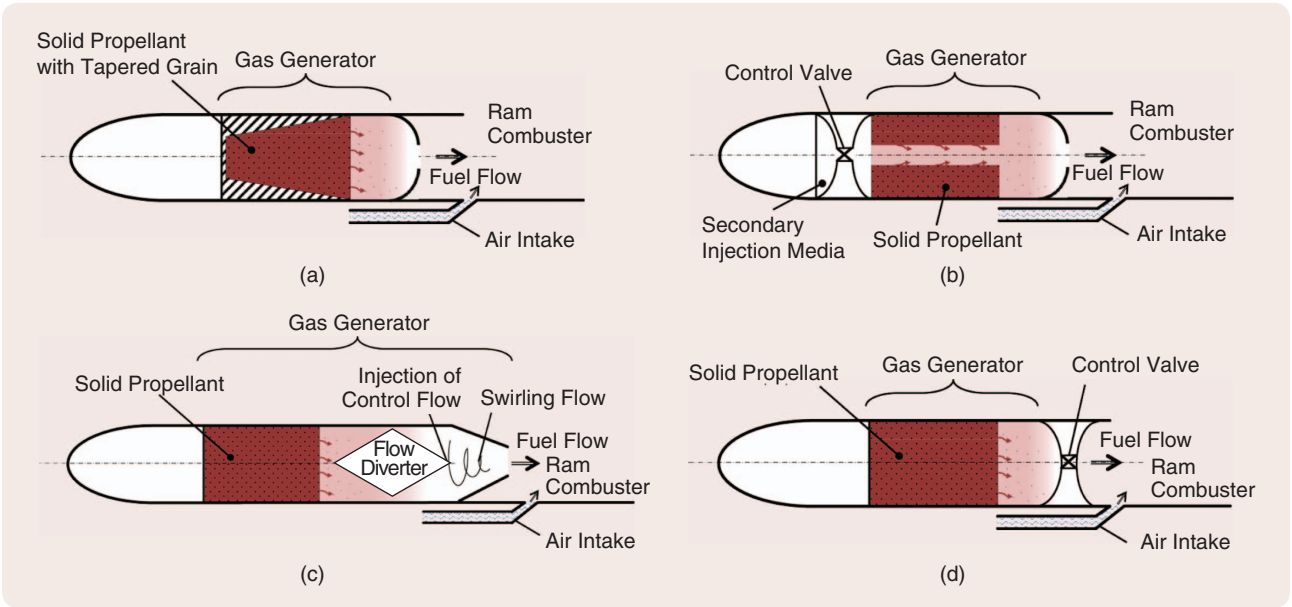

FIGURE 2 Methods of regulating the fuel flow rate from the gas generator to ram combustor (figures originated from [5] and [6], used with permission): (a) changing the burning area of the propellant, (b) using secondary injection, (c) using a vortex valve, and (d) using a control valve.

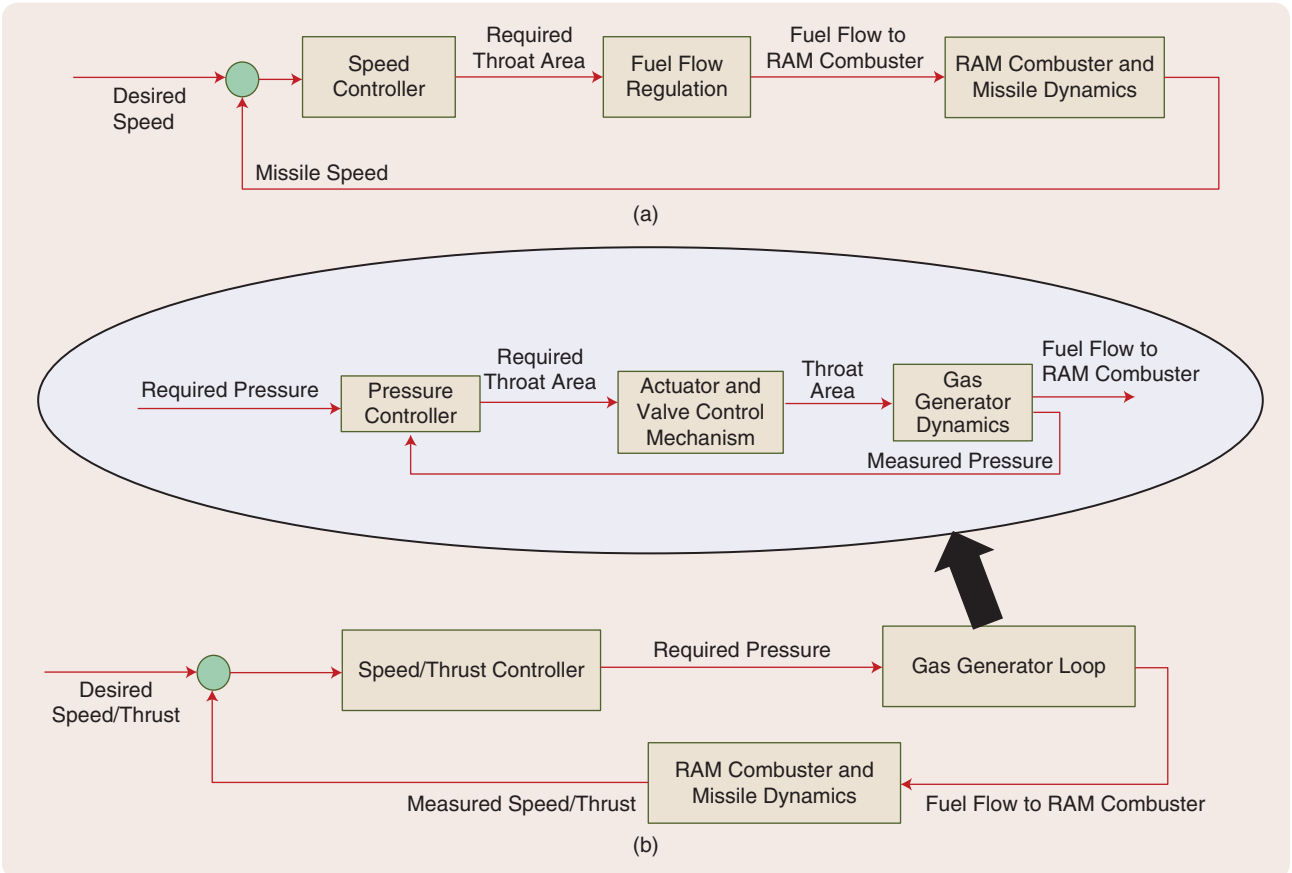

FIGURE 3 Alternative speed control loops of a throttleable ducted rocket. (a) The single speed or thrust loop, formed with the speed or thrust controller, that calculates the necessary throat area directly to set the missile speed equal to the desired speed, fuel flow regulation from the gas generator (GG) to the ram combuster, and combuster and missile dynamics. (b) The speed or thrust control loop hierarchical structure. The GG loop serves as an inner loop in this structure and is responsible for providing the required gas pressure inside (GG) that is dictated by the speed or thrust controller. The GG loop contains the pressure controller, actuator, valve mechanism, and GG dynamics. The output of the GG loop is the mass flow rate of the fuel.

pressure controller, which prevents undesired pressure buildup and possible structural damage. The GG pressure control loop in the second method is the focus of this article. It is shown here that seemingly separate tools, such as delay compensation, adaptation to uncertainties, and transient response improvement, can be combined to obtain solutions that can dramatically improve the performance of a challenging control loop, such as pressure control, over conventional approaches. Note that the nonminimum phase dynamics between the throat area and the fuel mass flow rate does not effect the inner pressure control loop and should be handled in the outer speed or thrust loop. This nonminimum phase dynamics is explained further in "Nonminimum Phase Behavior of Thrust in Throttleable Ducted Rockets."

The discussion in this article on the employment of advanced control methodologies should benefit practitioners whose goal is to obtain a fast system response in safety-critical applications where nonlinear dynamics, time-varying parameters, and time delays pose significant challenges. One of the most common approaches to control GG pressure is utilizing linear controllers that are designed based on a model of the system obtained by linearizing the nonlinear dynamics around a certain operating point [14], [16], [17]. Although this method is simple to implement, it may limit the performance when the operating point changes, as shown in the simulations and experimental studies presented in this article. Apart from the nonlinearities, another challenge for GG pressure control is that as the fuel burns, the free volume inside the GG increases with time, which makes the system time varying. Moreover, the GG dynamics contain several uncertainties emanating from metallic particles inside the solid fuel, such as deposition at the nozzle throat and ablation of mechanical elements. One of the more sophisticated control approaches to address these issues is gain scheduling [13], [15], where full knowledge of the controlled plant in the form of a high-fidelity mathematical model is employed to prepare lookup tables that are then used to assign appropriate controller gains at different operation modes and conditions. Another method, which is employed for the flight-performance evaluation study of the Meteor missile, is the performance funnel approach [18], [19], where a proportional controller is utilized with a time-varying gain

Nonminimum Phase Behavior of Thrust in Throttleable Ducted Rockets

When represented in the Laplace domain, a nonminimum phase system transfer function has unstable zeros, which means that at least one root of the numerator polynomial in the transfer function has positive real parts. Nonminimum phase behavior in the time domain manifests itself in the step response, where the response initially moves to the "wrong" direction before it eventually reverses direction and approaches its steady-state value.

In throttleable ducted rockets (TDRs), the relationship between the throat area and the fuel mass flow rate shows a nonminimum phase behavior. This does not affect the gas generator (GG) pressure control since, in the pressure loop, the feedback variable is the pressure inside the GG (see Figure 3). Therefore, this phenomenon should be addressed in the outer speed or thrust loop.

The dynamics of the nonminimum phase behavior in TDRs is demonstrated in Figure S1. Consider the case when the fuel flow rate generated inside the GG is equal to the ejected fuel flow rate. When there is a step increase in the throat area, it causes an instant discharge of the fuel, which increases the ejected mass flow rate instantly but decreases the pressure inside the medium. The burning rate of the solid propellant decreases due to its pressure sensitivity (it is known that the burning rate is affected by the pressure of the chamber [7], which is the pressure sensitivity of the propellant). This pressure sensitivity reduces the pressure to a lesser value. The mass flow rate coming out of the GG (assuming chocked flow conditions at the throat) is

$$\dot{m}_{\text{out}} = \frac{PA_t}{c^*}, \tag{S1}$$

where A_t is the throat area, P is the pressure, and c^* is the characteristic velocity of the fluid inside the GG. Therefore, the flow rate out of the GG eventually decreases. A step increase in the throat area initially increases but eventually decreases the mass flow rate of the ejected fuel, which indicates a nonminimum phase behavior.

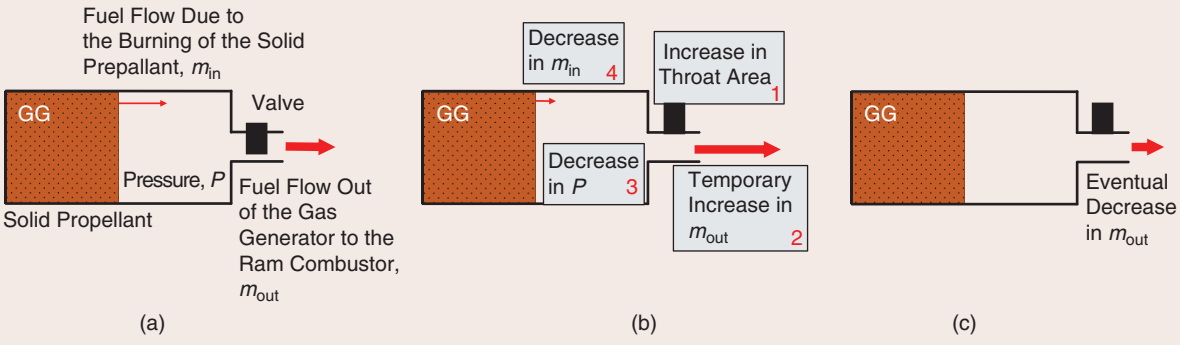

FIGURE S1 The nonminimum phase behavior of ejected fuel from the gas generator (GG). (a) shows the steady-state conditions. In (b), a positive step change in the throat area is given as an input to the system, which results in a temporary increase in the ejected mass flow rate and a decrease in the pressure inside the GG. The burning rate of the solid propellant decreases due to the decrease in pressure. In (c), after the transients are removed, the ejected mass fuel flow rate $\dot{m}_{\text{out}}$ reaches its reduced steady-state value due to lower burning rates. Hence, a step increase in the throat area initially increases the ejected flow rate, but then the flow rate eventually decreases, which is a nonminimum phase behavior.

that is adjusted online to keep the error of the closed-loop system within a predefined performance funnel. One practical disadvantage of funnel control is that, although the error stays inside a funnel, it does not guarantee the convergence to zero [20], which reduces the steady-state performance of the closed-loop system.

The final challenge considered in this article for gas pressure control is the time delay originating from pressure measurement, computational, and actuation delays and those inherent in system dynamics. The Smith predictor [21] is an early approach to addressing the time delay in control problems, where future prediction of the system output is used in the feedback that mitigates the destabilizing effects of the delay. The finite spectrum assignment method [22] and adaptive delay compensation tools are also developed [23]–[25]. Other notable studies on the adaptive control of time-delay systems are shown in [26] and [27], where unknown input delays and both state and input delays are addressed, respectively. Adaptive-loop recovery [28] is also shown to work well with the time delays of the flight-control problem. In addition, the extension of predictor feedback to nonlinear and delay-adaptive systems with actuator dynamics modeled by partial differential equations is discussed in [29]. A Pade-approximation-based approach for addressing the

time delay in actuators in the context of model reference adaptive control (MRAC) theory is addressed in [30] and [31]. It is shown that by reinforcing classical ideas from adaptive control literature with recent developments in delay compensation and transient performance improvement, the previously discussed control challenges can be addressed and a high-speed pressure response can be obtained in a safe manner by preventing excessive oscillations, without the need for precise system dynamics and the conservatism of robust approaches. Aside from pressure control problems, the benefits of combining delay compensation, adaptation, and transient response improvement methods can be realized in a variety of domains where uncertainties and time delays play a dominant role. Various adaptive delay compensation approaches have already been implemented in a wide array of plants, including teleoperation systems [32], internal combustion engines [33], [34], biology [35], [36], space systems [37], and transportation [38]. In this article, a unique combination of an adaptive delay compensation method [39] and adaptive transient performance improvement method [40]–[43] is discussed. The presented solution, termed the delay-resistant closed-loop reference model (DR-CRM) adaptive controller is investigated through simulations and experimental studies, where comparisons with progressively more sophisticated control approaches are carefully conducted.

In TDR research, cold-air test setup is widely considered the critical step in the validation of subsystems and methods. The setup is used, for example, to validate the numerical simulation results of flow characteristics, test the structures that are used to change the throat area, and characterize the materials that are planned for use in the construction [44]–[49]. A control algorithm is also a subsystem that must be qualified. This test setup conducts a comparative analysis of alternative control systems [50], which is then used to acquire a proper control methodology based on the gained insight. For the purposes of this article, Roketsan, Inc. provided its facilities to create an industrial-grade test setup that was utilized for the experimental studies.

The following sections present the nonlinear model of the system used for the discussions on alternative control approaches. The first principles for obtaining the initial model and enhancements through the use of experimental data are explained in detail. Moreover, the theory behind the DR-CRM adaptive controller is presented. Background material on this topic is provided in "Classical Model Reference Adaptive Control." In addition to the fundamental theory, practical concerns (such as drifting of the control parameters due to the controller's attempts to compensate for noise or unmodeled dynamics) and the determination of how fast to update the adaptive parameters are also discussed. Simulation and experimental implementation of the proposed control approach is presented. Depending on the mission, the desired pressure variations in TDRs can be small or large around several different operating regions. It is demonstrated that the investigated control solution prevents excessive pressure oscillations without slowing down the response of the system in all of the operating regions and pressure variation amplitudes that are tested.

BUILDING THE NONLINEAR MODEL THROUGH FIRST PRINCIPLES AND DATA

Conducting experiments at high pressures is both dangerous and expensive. Therefore, a high-fidelity plant model that can be used to test and tune alternative control approaches in the simulation environment is invaluable for the industry. A realistic model not only helps to minimize controller tuning time and effort in the experimental stage but also provides valuable insights on creating safe test scenarios (where the pressure is kept within allowable limits) that will protect the workers and system hardware. This section presents the procedures to obtain a reliable system model, which mainly consist of using the first principles to obtain an initial model and employing experimental data to improve model fidelity. A modeling procedure combining the first principles and experimental data can produce a high-fidelity model that is beneficial for controller testing in the simulation environment. However, this model can be unnecessarily complicated for the controller development. As will be presented in the later parts of this section, basic model simplification methods can be implemented to obtain a model for controller development.

Cold-air test setup consists of a control volume (pressure chamber), actuator, valve mechanism, pressure sensor, drivetrain elements, gas supply, and pressure regulator (see Figure 4). A continuous flow of gas is provided by a nitrogen source to the plant from the inlet, and the flow rate is adjusted by a pressure regulator. Besides its well-known characteristics, nitrogen is a safe (nonflammable at testing conditions and nontoxic) and inexpensive gas that can be easily obtained. The output of the model (which is the pressure inside the control volume) is controlled by changing the exit throat area of the flow. In the experimental setup in this article, the throat area is increased or decreased using the linear motion of a pintle, whose geometrical analysis is provided in this section. Another solution uses a piston-type valve. A comparative analysis of these two alternatives, together with a geometrical analysis of the latter, is provided in "Pintle Versus Piston." Drivetrain elements convert the rotational motion of the actuator (a brushless dc motor) to translational motion of the pintle with the required amount of reduction.

Pressure Dynamics

Assuming ideal gas conditions, the difference between the mass flow rates going into the control volume (pressure chamber) $\dot{m}_{\text{in}}$ [kg/s] and out of the control volume $\dot{m}_{\text{out}}$ [kg/s] is

$$\dot{m}_{\text{in}} - \dot{m}_{\text{out}} = \frac{\dot{P}V}{RT}, \tag{1}$$

Classical Model Reference Adaptive Control

Model reference adaptive control (MRAC) is commonly used for linear time-invariant systems with uncertain parameters. A brief introduction to this controller is provided for both a scalar and higher-order single-input, single-output system.

SCALAR CASE

Consider a first-order plant

$$\dot{x}(t) = ax(t) + bu(t), \tag{S2}$$

where $x \in \Re$ is the output, $u \in \Re$ is the input of the plant, and $a, b \in \Re$ are the plant parameters. In classical MRAC, the plant output is expected to track the output of a reference model (teacher). The closed-loop system specifications are enforced through this reference model. The reference model is defined as

$$\dot{x}_m(t) = a_m x_m(t) + b_m r(t), \tag{S3}$$

where $x_m, r \in \Re$ are the reference model output and a bounded command (reference) to the closed-loop system, respectively. a_m and b_m are the parameters that are chosen to specify the closed-loop system requirements. For this scalar case, it is sufficient to choose $a_m < 0$ to satisfy the necessary stability conditions for both the reference model and the overall closed-loop system. However, additional requirements must be satisfied for the higher-order case, which are explained in the section "Higher-Order Case."

The control problem is to find the controller

$$u(t) = \theta x(t) + kr(t), \tag{S4}$$

such that with the controller parameters $\theta, k \in \Re$, the tracking error $e_1(t) = x(t) - x_m(t)$ between the plant and the reference model outputs converges to zero. The control problem can easily be solved if the plant parameters a, b are known precisely. If the controller parameters are chosen as $\theta^* = (a_m - a)/b$ and $k^* = b_m/b$, then the closed-loop system dynamics become the same as those of the reference model. The existences of these ideal control parameters are the matching conditions. However, it is not always possible to determine the exact values of plant parameters a, b. In the design of MRAC, it is assumed that the plant parameters (and hence the ideal values of the controller parameters, θ^*, k^*) are unknown. Therefore, the control parameters are adjusted online in a unique way (which is explained below) to make the tracking error reach zero and maintain all the system signal stability. Controller parameter errors $\tilde{\theta}(t) = \theta(t) - \theta^*$ and $\tilde{k}(t) = k(t) - k^*$ are defined as the deviations of the real parameters $\theta(t), k(t)$ from their ideal values. Substituting (S4) into (S2), the closed-loop system becomes

$$\dot{x}(t) = a_m x(t) + b_m r(t) + b\tilde{\theta}(t)x(t) + b\tilde{k}(t)r(t). \tag{S5}$$

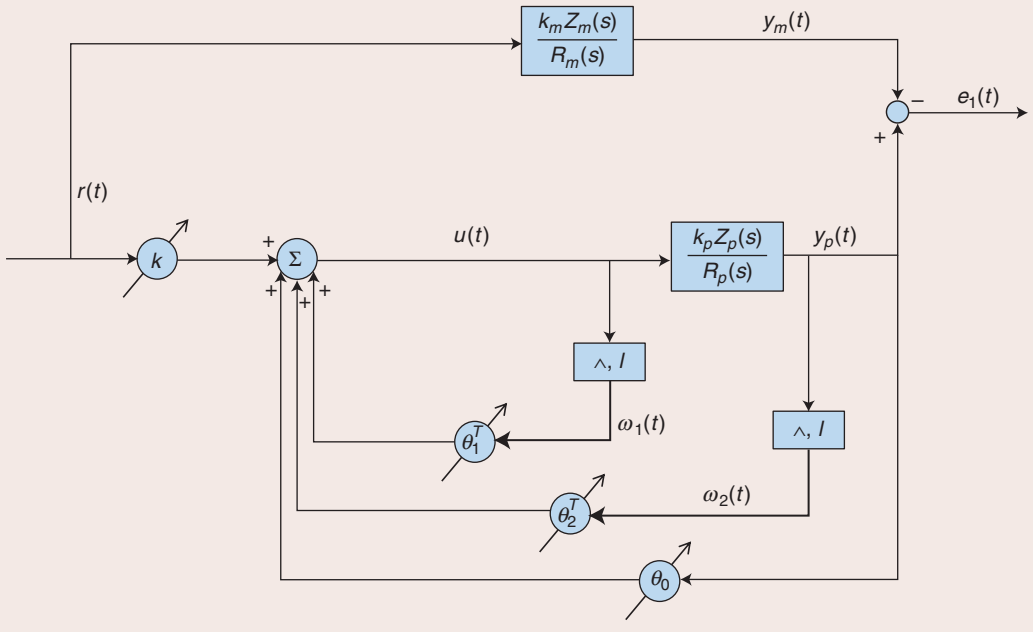

FIGURE S2 A model reference adaptive control (MRAC) structure, originated from [51]. Controller parameters $\theta_1^T(t), \theta_2^T(t), \theta_0(t)$, and $k(t)$ are updated online with the tracking error $e_1(t)$ between the plant output and reference model outputs.

To understand the error dynamics between the plant and reference model outputs in the presence of parameter errors, (S3) is subtracted from (S5) to obtain

$$\dot{e}_1(t) = a_m e_1(t) + b\tilde{\theta}(t)x(t) + b\tilde{k}(t)r(t). \tag{S6}$$

Error dynamics can be analyzed using a Lyapunov function candidate

$$V(e_1, \tilde{\theta}, \tilde{k}) = \frac{1}{2}e_1^2 + \frac{b}{2\,\mathrm{sgn}(b)\gamma_1}\tilde{\theta}^2 + \frac{b}{2\,\mathrm{sgn}(b)\gamma_2}\tilde{k}^2, \tag{S7}$$

where $\mathrm{sgn}(\cdot)$ is the signum function and γ_1, γ_2 are positive constant scalars. Using the derivative of the Lyapunov function candidate and (S6) gives

$$\dot{V} = a_m e_1^2 + \left(xe_1 + \frac{\dot{\tilde{\theta}}}{\mathrm{sgn}(b)\gamma_1}\right)b\tilde{\theta} + \left(re_1 + \frac{\dot{\tilde{k}}}{\mathrm{sgn}(b)\gamma_2}\right)b\tilde{k}. \tag{S8}$$

If the adaptation laws to update the controller parameters are chosen as

$$\begin{aligned}\dot{\tilde{\theta}}(t) &\equiv \dot{\theta}(t) = -\gamma_1\,\mathrm{sgn}(b)e_1(t)x(t)\\ \dot{\tilde{k}}(t) &\equiv \dot{k}(t) = -\gamma_2\,\mathrm{sgn}(b)e_1(t)r(t),\end{aligned} \tag{S9}$$

then $\dot{V} \le 0$ and the boundedness of all signals in the system are ensured. Furthermore, since $\ddot{V} = 2a_m e_1 \dot{e}_1$ is also bounded, $e_1 \to 0$ as $t \to \infty$ from Barbalat's Lemma [S1].

HIGHER-ORDER CASE

Consider the case of a single-input, single-output linear plant with a transfer function of order larger than one and a relative order equal to one.

Definition 1

A transfer function $G(s)$ is called a strictly positive real (SPR) transfer function if it satisfies the following criteria:

- $G(s)$ is stable.
- $Re[G(i\omega)] > 0$ for $\omega > 0$.
- $G(\infty) > 0$.

Lemma 1 [51], [S1]

Consider the dynamical system described by

$$\begin{aligned}\dot{x}(t) &= Ax(t) + b\phi^T(t)w(t),\\ y(t) &= h^T x(t),\\ z_1(t) &= ky(t),\end{aligned} \tag{S10}$$

where k is an unknown constant whose sign is known, the pair (A, b) is stabilizable, (h^T, A) is detectable, and the transfer function $H(s) = h^T(sI - A)^{-1}b$ is SPR. In addition, the scalar $z_1(t)$ and vector $w(t)$ can be measured. Under these conditions, if the adjustable parameter $\phi(t)$ is updated using the adaptive law

$$\dot{\phi}(t) = -\,\mathrm{sgn}(k)z_1(t)w(t), \tag{S11}$$

then the equilibrium point $x = 0, \phi = 0$ is uniformly stable in the large. Furthermore, if ω is bounded, then $x(t)$ converges to zero asymptotically.

Consider the plant dynamics described by the following state-space representation

$$\begin{aligned}\dot{x}_p &= A_p x_p + b_p u,\\ y_p &= h_p^T x_p,\end{aligned} \tag{S12}$$

where x_p is an n-dimensional state vector, u is the scalar control input, and y is the scalar plant output. The matrix A_p and vectors b_p and h_p are assumed to be unknown. The transfer of this plant is

$$\frac{Y_p(s)}{U(s)} = k_p\frac{Z_p(s)}{R_p(s)} = h_p^T(sI - A_p)^{-1}b_p. \tag{S13}$$

It is assumed that all of the roots of the numerator polynomial $Z_p(s)$ have negative real parts. This is required to prevent the possibility of an unstable pole zero cancellation.

The state-space representation of the nth-order reference model is

$$\begin{aligned}\dot{x}_m &= A_m x_m + b_m r\\ y_m &= h_m^T x_m,\end{aligned} \tag{S14}$$

with the associated transfer function

$$W_m(s) \equiv \frac{Y_m(s)}{R(s)} = k_m\frac{Z_m(s)}{R_m(s)} = h_m^T(sI - A_m)^{-1}b_m. \tag{S15}$$

Equation (S15) of the reference model is selected to be SPR, and the need for this requirement will become apparent in the following. The gain k_m is assumed to be positive for simplicity. The MRAC controller structure that makes the error $e_1 = y_p - y_m$ converge to zero is given in Figure S2. Using the variables in the figure, the equations describing the controller dynamics are

$$\begin{aligned}\dot{\omega}_1(t) &= \Lambda\omega_1(t) + lu(t),\\ \dot{\omega}_2(t) &= \Lambda\omega_2(t) + ly_p(t),\\ \omega(t) &\equiv [r(t), \omega_1^T(t), y_p(t), \omega_2^T(t)]^T,\\ \theta(t) &\equiv [k(t), \theta_1^T(t), \theta_0(t), \theta_2^T(t)]^T,\\ u(t) &= \theta^T(t)\omega(t),\end{aligned} \tag{S16}$$

where $\Lambda \in \Re^{(n-1)\times(n-1)}$ is a matrix with eigenvalues that have negative real parts and the pair (Λ, l) is controllable.

The first step in designing the MRAC is to show the existence of a fixed (nonadaptive) controller that will ensure that the closed-loop transfer function becomes equal to the transfer function of the reference model. In this regard, assuming a fixed control parameter gain vector θ_f, the following definitions can be made:

$$\frac{C(s)}{\lambda(s)} \equiv \theta_{1f}^T(sI - \Lambda)^{-1}l, \quad \frac{D(s)}{\lambda(s)} \equiv \theta_{0f} + \theta_{2f}^T(sI - \Lambda)^{-1}l. \tag{S17}$$

Note that the degree of the polynomials $\lambda(s)$, $C(s)$, and $D(s)$ are $(n-1), (n-2)$, and $(n-1)$, respectively. Using (S17), the overall closed-loop transfer function (assuming fixed controller gains) is

$$W(s) \equiv \frac{Y_p(s)}{R(s)} = \frac{k_f k_p Z_p(s)\lambda(s)}{(\lambda(s) - C(s))R_p(s) - k_p Z_p(s) D(s)}. \quad \text{(S18)}$$

Ideal fixed control parameter values $k^*, \theta_1^{*T}, \theta_2^{*T}$, and θ_0^* can be selected to make the closed-loop transfer function (S18) equal to the reference model transfer function (S15). Note that Λ can be selected such that $\lambda(s) = Z_m(s)$ [see (S17)] . Also, $C(s)$ can be shaped using θ_{1f}, and $D(s)$ can be shaped using θ_{0f} and θ_{2f}. Therefore, there exist certain ideal values, θ_1^*, θ_2^*, and θ_0^* for these fixed parameters such that when $\theta_{1f} = \theta_1^*, \theta_{2f} = \theta_2^*$, and $\theta_{0f} = \theta_0^*$, both

$$\lambda(s) - C(s) = Z_p(s) \text{ and } R_p(s) - k_p D(s) = R_m(s) \quad \text{(S19)}$$

are satisfied. Finally, k_f can be selected such that $k_f = k^* = k_m/k_p$. It can then be verified that with these fixed values, the closed-loop transfer function (S18) becomes equal to the reference model transfer function (S15).

Having established the existence of the ideal control parameters to make the closed-loop transfer function equal to the reference model transfer function, the second step of the controller design can be introduced. However, note that the value of the ideal parameters are not known because plant parameters are unknown. Even though the ideal parameters are unknown, it can be shown that, with certain online adaptation mechanisms, they can be adjusted in such a way that the tracking error approaches zero while keeping all system signals bounded. To demonstrate how this is achieved, the dynamics of the plant and controller are first rewritten using (S12) and (S16) as

$$\begin{aligned} \dot{x}_p(t) &= A_p x_p(t) + b_p(\theta^T(t)\omega(t)), \\ \dot{\omega}_1(t) &= \Lambda\omega_1(t) + l(\theta^T(t)\omega(t)), \\ \dot{\omega}_2(t) &= \Lambda\omega_2(t) + l(h_p^T x_p(t)). \end{aligned} \quad \text{(S20)}$$

Using the definitions $\tilde{k}(t) \equiv k(t) - k^*, \tilde{\theta}_1(t) \equiv \theta_1(t) - \theta_1^*, \tilde{\theta}_0(t) \equiv \theta_0(t) - \theta_0^*, \tilde{\theta}_2 = \theta_2(t) - \theta_2^*$ and $\phi(t) = [\tilde{k}(t), \tilde{\theta}_1^T(t), \tilde{\theta}_0(t), \tilde{\theta}_2^T(t)]$, (S20) can be rewritten as

$$\begin{aligned} \dot{x} &= A_{mn}x + b_{mn}[\phi^T\omega + k^* r], \\ y_p &= h_{mn}^T x, \end{aligned} \quad \text{(S21)}$$

where $x = [x_p^T, \omega_1^T, \omega_2^T]^T$ and

$$A_{mn} = \begin{bmatrix} A_p + b_p\theta_0^* h_p^T & b_p\theta_1^{*T} & b_p\theta_2^{*T} \\ l\theta_0^* h_p^T & \Lambda + l\theta_1^{*T} & l\theta_2^{*T} \\ l h_p^T & 0 & \Lambda \end{bmatrix}, \; b_{mn} = \begin{bmatrix} b_p \\ l \\ 0 \end{bmatrix}, \; h_{mn} = \begin{bmatrix} h_p \\ 0 \\ 0 \end{bmatrix}. \quad \text{(S22)}$$

If the control parameters $\theta(t)$ become equal to their ideal values θ^*, then the closed-loop transfer function becomes equal to the reference model transfer function. Therefore, using (S21) and the fact that the control parameter deviation vector ϕ becomes identically zero, the reference model can be represented by

$$\begin{aligned} \dot{x}_{mn} &= A_{mn}x_{mn} + b_{mn}k^* r, \\ y_m &= h_{mn}^T x_{mn}, \end{aligned} \quad \text{(S23)}$$

where $x_{mn} = [x_p^{*T}, \omega_1^{*T}, \omega_2^{*T}]$. It is noted that x_{mn} consists of the ideal states in the reference model corresponding to the closed-loop system states $x_p(t), \omega_1(t)$, and $\omega_2(t)$. The reference model transfer function (S15) is nth order and (S23) is $(3n-2)$th order. Therefore, (S23) is a nonminimal state-space representation of the reference model. Defining the errors $e \equiv x - x_{mn}$ and $e_1 \equiv y_p - y_m$ and subtracting (S23) from (S21) yields

$$\begin{aligned} \dot{e}(t) &= A_{mn}e(t) + b_{mn}\phi^T(t)\omega(t), \\ e_1(t) &= h_{mn}^T e(t). \end{aligned} \quad \text{(S24)}$$

Lemma 1 illustrates that, if the controller parameters are adjusted online by employing the following adaptation rules, then all of the system signals will be bounded and the tracking error e_1 will converge to zero

$$\begin{aligned} \dot{k}(t) &= -\operatorname{sgn}(k_p)\gamma_k e_1(t) r(t), \\ \dot{\theta}_0(t) &= -\operatorname{sgn}(k_p)\gamma_0 e_1(t) y_p(t), \\ \dot{\theta}_1(t) &= -\operatorname{sgn}(k_p)\gamma_1 e_1(t)\omega_1(t), \\ \dot{\theta}_2(t) &= -\operatorname{sgn}(k_p)\gamma_2 e_1(t)\omega_2(t), \end{aligned} \quad \text{(S25)}$$

where $\gamma_k, \gamma_0, \gamma_1$, and γ_2 are positive constants that define the speed of adaptation. These variables are also called adaptation rate parameters. A more detailed discussion and the extension for more general classes of plants can be found in [51].

REFERENCE

[S1] J.-J. E. Slotine and W. Li, *Applied Nonlinear Control*. Eagle Wood Cliffs, NJ: Prentice-Hall, 1991.

where R [J/(kg-K)] is the specific gas constant and P [Pa], T [K], and V [m^3] are the pressure, temperature, and volume of the gas inside the control volume. Assuming an isothermal process with no change in the control volume, then $\dot{V} = \dot{T} = 0$.

The mass flow out of the control volume is a function of the throat area (A_t[mm^2]) and the pressure inside the control volume (P). Assuming chocked flow conditions, the relationship between the throat area and resulting mass flow rate out of the control volume can be calculated as [13]

$$\dot{m}_{\text{out}} = PA_t\left(\left(\frac{2}{\gamma+1}\right)^{\left(\frac{\gamma}{\gamma-1}\right)}\right)\sqrt{\frac{\gamma}{RT^*}} = \frac{PA_t}{c^*}, \quad (2)$$

where γ is the specific heat ratio of air, T^* is the temperature at the throat, and c^* [m/s] is the characteristic velocity of the gas inside the control volume. Using (1) and (2) yields

$$\dot{P} = c_1\dot{m}_{\text{in}} - c_2 PA_t = M - c_2 PA_t, \quad (3)$$

where $c_1 = (RT)/V, c_2 = c_1/c^*$, and $M = c_1\dot{m}_{\text{in}}$.

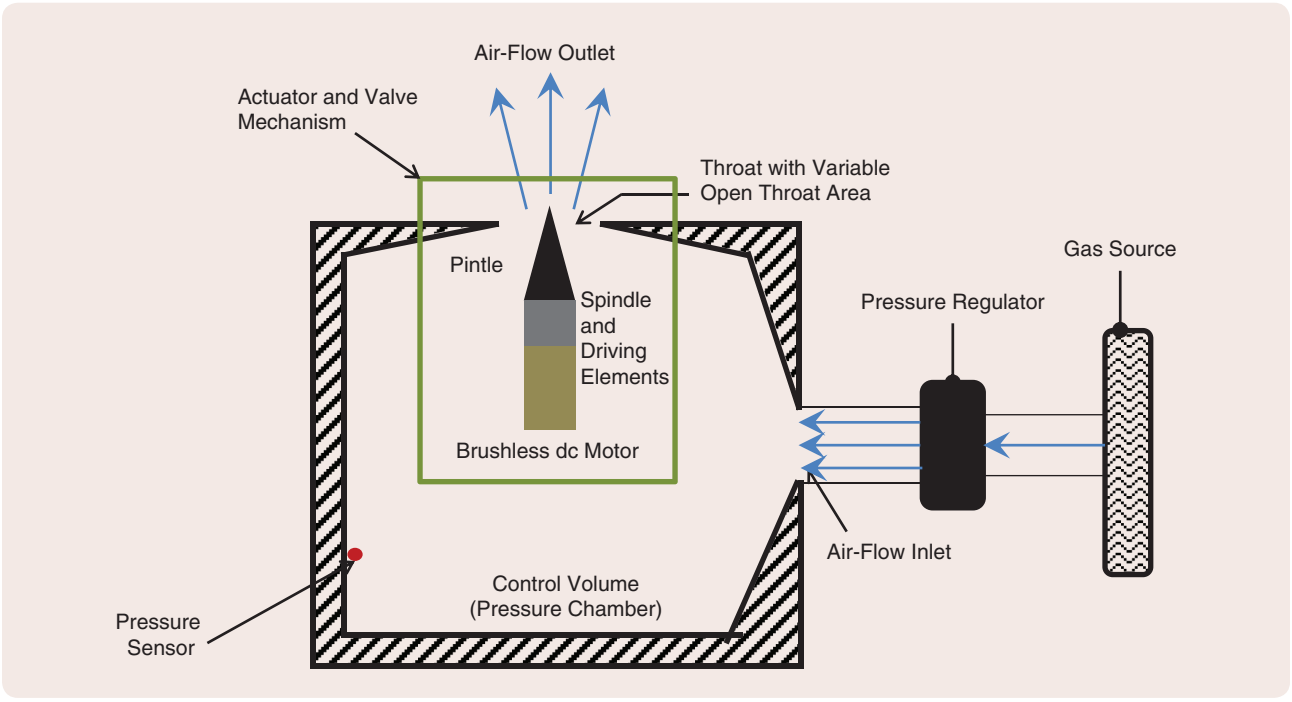

FIGURE 4 A schematic of the cold-air test setup. The overall cold-air test setup consists of a pressure chamber, an actuator, a valve mechanism, a pressure sensor, drivetrain elements, a gas supply, and a pressure regulator. A continuous stream of gas (supplied by the gas source and regulated by the pressure regulator) fills the pressure chamber, which has inlet and outlet ports. The control valve at the exit port is used to control the gas pressure inside the chamber.

Actuator Dynamics

In the experimental setup built by Roketsan, Inc., a brushless dc motor is used as the actuator. The motor is run in position control mode, and an encoder is used to measure the position or speed of the rotor. A first-order dynamic is sufficient enough to model this architecture

$$W_{\text{act}}(s) = \frac{\theta_{\text{mes}}(t)}{\theta_{\text{com}}(t)} = \frac{1}{\tau_{\text{act}} s + 1}, \tag{4}$$

where θ_{mes} [quadrature] is the measured actual rotational position of the rotor, θ_{com} [quadrature] is the commanded rotational position (4000 quadratures correspond to one rotation), and θ_{act} is the actuator closed-loop time constant.

Valve Geometry and Drivetrain Elements

The drivetrain elements consist of a gear box and a ball screw spindle to convert the rotational motion of the motor into the translational motion of a pintle at the throat area (see Figure 5). The linear position of the pintle determines the throat opening.

The pintle has one degree of freedom in the x-direction and open throat area changes as the pintle moves along the x-axis due to its conical surface. The cross-sectional area of the cylindrical part at the back of the pintle is smaller than the fixed throat area, which ensures that the open throat area A_t is always larger than zero and protects the system from rapid pressure build up. The valve and the drive train models are explained next.

Valve Geometry

There exists a complex relationship between the movement of the pintle and the minimum throat area, where the choked flow conditions occur, due to their complex geometries [44], [46]. The size and location of the minimum throat area is hard to estimate analytically because that location of the choked flow line, where the throat area is minimum, shifts toward the upstream as the pintle moves into the throat [46]. The size of the open throat area can be approximated as the projection of the real area on the vertical surface that is perpendicular to the pintle center line. Movement of the pintle along the x-axis reduces the projected throat area by

$$y = y_0 - \tan(\alpha)x, \tag{5}$$

where y_0 is the radius of the pintle at the cylindrical base and α is the half of the cone angle at the tip (see Figure 5). The projected open throat area is then calculated as

$$A_t = (r_0^2 - y^2)\pi. \tag{6}$$

Drivetrain Elements

In the experimental setup, a gear box with a reduction ratio of $1:R_1$ (multiplying the torque output of the actuator by $R1$) is used. Moreover, a ball screw spindle is present, which is a mechanical element with a threaded shaft and outer nuts and balls in between. Rotational motion of its

Pintle Versus Piston

In throttleable ducted rocket (TDR) control, the variable thrust is realized by adjusting the mass flow rate discharged to the ram combustor, which is achieved by altering the throat area between the gas generator (GG) and the ram combustor. The throat area is manipulated by restricting the area using mechanical elements, one of which is a piston [see Figure S3(a) and (b)] (which is inserted perpendicular to the flow) and the other is a pintle [see Figure S3(c)] (which is inserted parallel to the flow).

The pintle has several advantages over the piston. First, the piston has higher sensitivity, which is defined as the effect of one unit of movement on the resultant throat area change. Decreasing the conical angle increases the sensitivity even more. In addition, the radius of the cylindrical part at the back of the pintle can be chosen to be smaller than the radius of the throat, which results in movement without any hard stops and provides safer operation in case of a malfunction. There are also several disadvantages of the pintle, compared to the piston. First, the pintle geometry is more prone to degeneration due to operating conditions. The flow from the GG to the ram combustor has a very high temperature and contains metallic particles to enhance the combustion efficiency. This may spoil its prescribed shape and introduce disturbance. In addition, the pintle actuation subsystem must be located inside the GG, which makes the mechanical design problem more complex due to harsh conditions in the GG. The actuation subsystem also decreases the volume of the GG.

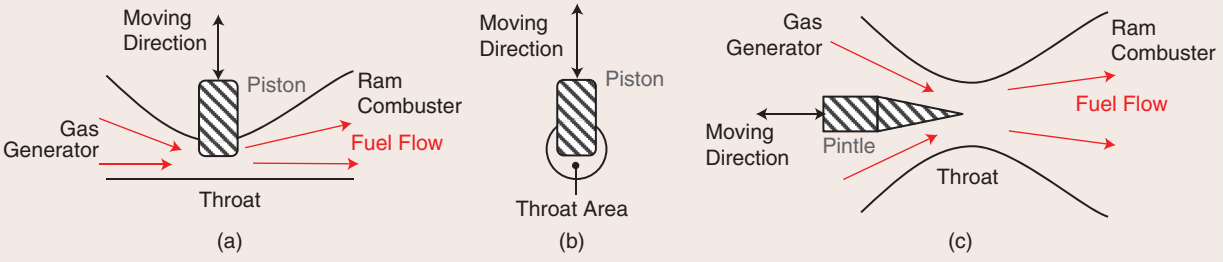

FIGURE S3 Different mechanical elements for throat area change (the figures originated from [5], used with permission). (a) and (b) show the operation of the piston-type structure utilized in the throat area change. By moving the piston linearly perpendicular to the flow, it is possible to have a more robust throat area changing system against harsh operating conditions. (c) shows the pintle-type element to change the throat area. Although high-sensitivity values can be achieved with this method, it is not appropriate for harsh operating conditions.

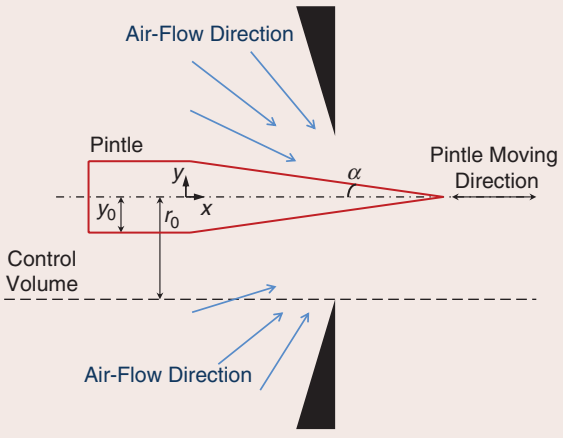

FIGURE 5 Valve geometry. This specific geometry is assigned to alter the effective throat area of the exit port of the pressure chamber in the cold-air test setup. The linear position of the conical pintle, which is controlled by an actuator, dictates the effective throat area.

shaft is transferred to the translational motion of the nut with high efficiency, due to its balls moving along the threads with low friction. The spindle used in this setup has an R_2-mm thread pitch. This means that one turn of rotational motion is converted to R_2-mm translational motion. Therefore, the relationship between the actuator rotational position, θ (quadrature), and the linear position of the pintle x (mm), can be calculated as

$$x = \frac{\theta R_2}{R_1 \times 4000}, \tag{7}$$

where 4000 quadratures correspond to one rotation.

Combining (5)–(7), the nonlinear relationship between the throat area and actuator angular position can be expressed as

$$A_t = (a_1 + a_2\,\theta + a_3\,\theta^2)\,\pi, \tag{8}$$

where $a_1 = r_0^2 - y_0^2$, $a_2 = 2y_0 \tan(\alpha) R_2 / (R_1 \times 4000)$ and $a_3 = -(\tan(\alpha) R_2 / (R_1 \times 4000))^2$.

Increasing Model Fidelity Using Experimental Data

As discussed earlier, a high-fidelity model is valuable for providing a relatively cheap and simple platform to test, compare, and validate alternative control approaches before the actual implementation. In this article, experimental data to enhance the system model developed using the first principles is presented. First, the actuator model is updated. The brushless dc motor is commanded to track inputs in the position controller mode, and based on the response of the actuator, the time constant τ_{act} in (4) is updated. Experiments also reveal that a considerable amount of time delay exists in the actuator control loop, which is due to the communication and computation lags. After adjusting the time constant and incorporating a time delay, the enhanced actuator model output is compared with the experimental results, and the outcomes are presented in Figure 6, which shows that the updated model has good agreement with the test data. To further improve the system model, the parameters in (3) are considered next. R, T, V, and c^* are available for the test conditions with good accuracy, and the values of these parameters are easily obtained. However, the mass flow rate ($\dot{m}_{in}$) is not always feasible to measure, especially for relatively small flow rate values. Therefore, the mass flow rate is calculated via (3) using the steady-state pressure values at different operating points and corresponding throat areas. Several values for $\dot{m}_{in}$ at different operating points are plotted in Figure 7 together with a polynomial fit. At low plant pressures, mass flow rates are nearly constant. However, mass flow rate decreases at higher pressures because high back pressure overcomes the mechanical force in the pressure regulator and reduces the flow rate. Using the polynomial that is fitted to the data in Figure 7, (3) is updated as

$$\dot{P} = c_1(c_3P^3 + c_4P^2 + c_5P + c_6) - c_2PA_t. \tag{9}$$

Open-loop simulation results with the overall updated system model along with experimental results (which are obtained for a range of operating points) are given in Figure 8. Note that the model enhancements can be further improved by making comparisons at several other operating points followed by further tuning of the parameters. However, this level of fidelity is enough for simulation evaluations of the controllers discussed in this article.

Modeling for Controller Design

The nonlinear model presented in the previous section evaluates controller alternatives in the simulation environment. To facilitate the controller design, a simpler model that is sufficiently accurate for developing controllers can be obtained

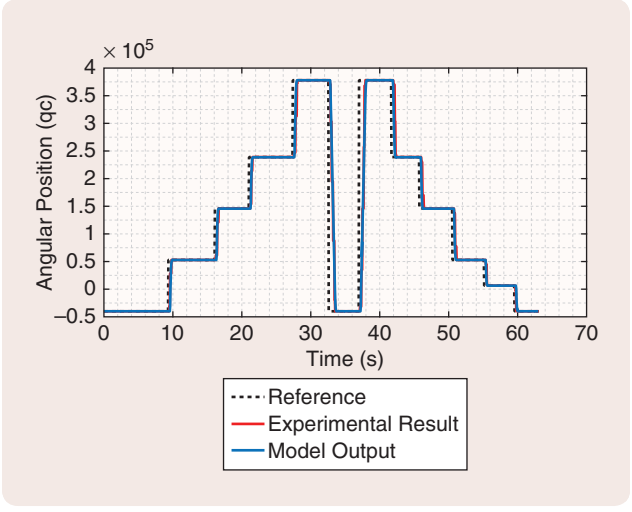

FIGURE 6 A comparison of the experimental and updated model results of the actuator. First, experimental results are obtained and then numerical simulations are created to obtain a good match by updating the actuator with the time constant τ_{act} in (4).

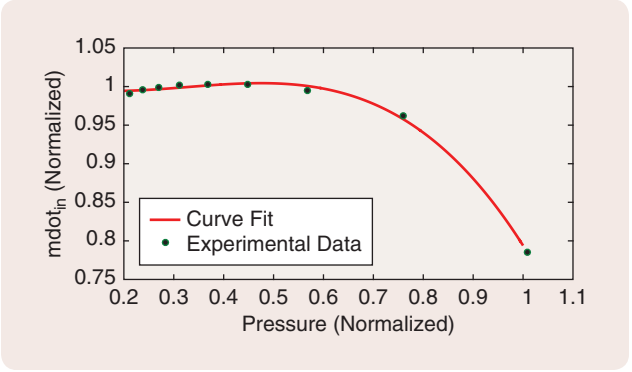

FIGURE 7 $\dot{m}_{in}$ in the experiments is curve fitted to the data (9). $\dot{m}_{in}$ data are calculated via (3) using steady-state pressure values at different operating points and corresponding throat areas, which are dictated manually. A third-order polynomial is fitted to the experimental data. Although mass flow rates are nearly constant at low plant pressures, they decrease at higher pressures because the pressure in the chamber acts like a back pressure for the pressure regulator, and high back pressure overcomes the mechanical force in the regulator and reduces the flow rate.

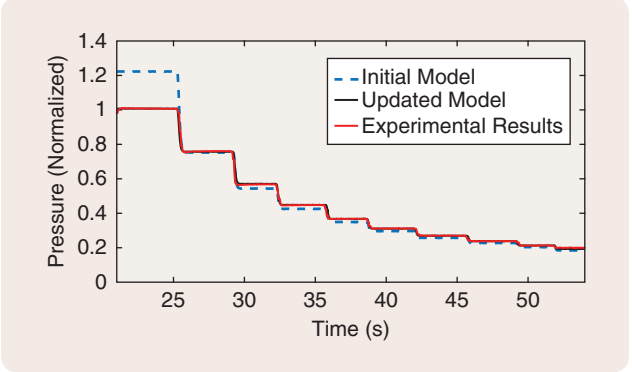

FIGURE 8 A comparison of the open-loop responses of the experimental setup and simulation with the initial (3) and updated plant models (9). The updated model shows a good match with the experimental data. The initial model, based on the constant mass flow rate at the inlet port, fails at high chamber pressures.

by linearizing the nonlinear plant model and valve equation in (3) and (8), respectively, and ignoring the actuator dynamics due to small time constants, compared to that of the pressure dynamics. Linearizing (3) around an equilibrium point $(P, A_t) = (P_0, A_{t0})$ yields

$$\dot{P} = \Delta\dot{P} = (-c_2 A_{t0})\Delta P - (c_2 P_0)\Delta A_t, \tag{10}$$

where $\Delta P = P - P_0$ and $\Delta A_t = A_t - A_{t0}$. Defining $a_p \equiv -c_2 A_{t0}$ and $b_p \equiv -c_2 P_0$, (10) can be rewritten as

$$\Delta\dot{P} = a_p \Delta P + b_p \Delta A_t. \tag{11}$$

The value of a_3 in (8) is much smaller than a_1 and a_2 for meaningful physical parameters, and therefore (8) can be approximated as

$$A_t \approx (a_1 + a_2\,\theta)\pi. \tag{12}$$

It is noted that the valve equation (12) converts the required throat area determined by the pressure controller to the required actuator rotational position, which is provided to the actuator/valve control mechanism as a reference (see Figure 3).

Therefore, together with the actuator time lag τ, the system model used to develop the controller can be determined as

$$W_p(s) = \frac{\Delta P(t)}{\Delta A_{t,\mathrm{com}}(t)} = \frac{b_p e^{-s\tau}}{s - a_p}. \tag{13}$$

THEORY: COMBINING ADAPTIVE DELAY COMPENSATION WITH ADAPTIVE TRANSIENT PERFORMANCE IMPROVEMENT

This section presents the theory behind the controller-termed DR-CRM adaptive controller, which combines delay compensation and adaptive transient performance improvement. "Classical Model Reference Adaptive Control" and "Closed-Loop Model Reference Adaptive Control" build on a basic knowledge of control theory to provide the background material necessary to grasp the main ideas of adaptation and transient performance improvement.

Consider the plant with an input time delay given as

$$y_p(t) = k_p \frac{Z_p(s)}{R_p(s)} u(t-\tau) = W_p(s)\,u(t-\tau), \tag{14}$$

where $y_p \in \Re$ is the measured output, $u \in \Re$ is the control signal, τ is the known time delay, and $Z_p(s)$ and $R_p(s)$ are monic coprime polynomials with orders of m and n, respectively. A monic polynomial is one that has the coefficient of one for its highest power term. Coprime polynomials do not share a common root. $k_p \in \Re$ is the constant gain of the plant. It is noted that the Laplace variable s in (14) is the derivative operator. Similarly, $1/s$ is the integral operator. The following assumptions are made for the plant:

- System order n is known and the relative degree $n^* = n - m = 1$.
- The sign of k_p is known.
- Polynomial $Z_p(s)$ is Hurwitz.

The first and the second assumptions are needed in the technical stability proof of the controller and hold true for a large class of systems. The last assumption is required to eliminate any unstable pole-zero cancellation. The reference model dynamics are given with the closed-loop reference model structure as

$$\begin{aligned} \dot{x}_m(t) &= A_m x_m(t) + b_m r(t-\tau) + L(y_p(t) - y_m(t)), \\ y_m(t) &= h_m^T x_m(t), \end{aligned} \tag{15}$$

where $x_m \in \Re^n$ is the state vector, $y_m \in \Re$ is the output, and $r \in \Re$ is the reference input for the reference model. $A_m \in \Re^{n\times n}$ and $b_m, L, h_m \in \Re^n$ are the state matrix, input vector, and feedback gain of the reference model and output vector, respectively. Using the Laplace transform, the input–output relationship of the closed-loop reference model can be obtained from (15) as

$$y_m(t) = W_m(s)\,r(t-\tau) + W_L(s)\,e_1(t), \tag{16}$$

where $e_1 = y_p - y_m$ is the tracking error and transfer functions are calculated as

$$\begin{aligned} W_m(s) &\equiv h_m^T (sI - A_m)^{-1} b_m = k_m \frac{Z_m(s)}{R_m(s)}, \\ W_L(s) &\equiv h_m^T (sI - A_m)^{-1} L = k_L \frac{Z_L(s)}{R_m(s)}. \end{aligned} \tag{17}$$

In (17), $R_m(s)$ is a monic polynomial with order n, while $Z_m(s)$ and $Z_L(s)$ are two monic polynomials with order $n-1$. $k_m \in \Re$ and $k_L \in \Re$ are the gains of the transfer functions.

Note that under model matching conditions [which is the case when a fixed (nonadaptive) controller is designed to make the closed-loop transfer function equal to the reference model transfer function $W_m(s)$], the tracking error e_1 becomes zero, which reduces the reference model (16) to

$$y_m(t) = W_m(s)\,r(t-\tau). \tag{18}$$

A fixed controller to achieve the model matching condition cannot be designed in the presence of plant uncertainties, since uncertainties are unknown by definition. However, as explained in "Classical Model Reference Adaptive Control" and "Closed-Loop Model Reference Adaptive Control," in the development of the controllers, the existence of such a controller must be ensured, even though the exact values of the control parameters are unknown.

The state-space description of the plant (14) and the signal generators for the output feedback problem with the controllable (F, g) pair are given as

Closed-Loop Model Reference Adaptive Control

Higher adaptation rates in adaptive laws (S9) and (S25) increase the speed of adaptation. However, it is observed in simulations and experiments that excessively increasing the adaptation rates causes undesired oscillations. To address this trade-off, the reference model is modified to obtain better transients [40], [S2]–[S9]. Closed-loop model reference (CRM) adaptive control is one of these methods, proposed in [41]–[43], [S10], [S11], which introduces an error feedback modification of the reference model to suppress the oscillations for higher adaptation rates (see Figure S4).

Consider the state-space representation of the reference model dynamics (S14) used in the classical model reference adaptive control (MRAC), given as

$$\begin{aligned} \dot{x}_m(t) &= A_m x_m(t) + b_m r(t), \\ y_m(t) &= h_m^T x_m(t). \end{aligned} \tag{S26}$$

As shown in "Classical Model Reference Adaptive Control," A_m, b_m, and h_m in classical MRAC are chosen such that the transfer function $W_m(s) \equiv h_m^T(sI - A_m)^{-1}b_m = k_m(Z_m(s)/R_m(s))$ becomes strictly positive real (SPR). In CRM adaptive control, the reference model is modified as

$$\begin{aligned} \dot{x}_m(t) &= A_m x_m(t) + b_m r(t) + L(y_p(t) - y_m(t)), \\ y_m(t) &= h_m^T x_m(t), \end{aligned} \tag{S27}$$

where $L \in \Re^n$ is the error feedback gain vector. The relationship between the reference model output y_m, the reference r, and the tracking error $e_1 = y_p - y_m$ then becomes

$$y_m(t) = W_m(s)r(t) + W_L(s)e_1(t), \tag{S28}$$

where

$$\begin{aligned} W_m(s) &\equiv k_m \frac{Z_m(s)}{R_m(s)} = h_m^T(sI - A_m)^{-1}b_m, \\ W_L(s) &\equiv k_L \frac{Z_L(s)}{R_m(s)} = h_m^T(sI - A_m)^{-1}L. \end{aligned} \tag{S29}$$

Note that in (S28), the Laplace variable s is the derivative operator. Similarly, $1/s$ is the integral operator. In CRM adaptive control, there is no modification on the controller structure (S16); therefore, the closed-loop dynamics can again be represented by (S20)–(S22). However, since the CRM reference model has an additional error feedback term, the procedure to show stability differs slightly from the MRAC. In this regard, consider the case when the controller parameters become equal to their ideal values, which means that $\phi = 0$ in (S21). In this case, the ideal closed-loop dynamics become

$$\begin{aligned} \dot{x}_{mn} &= A_{mn}x_{mn} + b_{mn}k^* r, \\ y_m &= h_{mn}^T x_{mn}, \end{aligned} \tag{S30}$$

where A_{mn}, b_{mn}, and h_{mn} are given in (S22) and $x_{mn} = [x_p^{*T}, \omega_1^{*T}, \omega_2^{*T}]$.

It was shown for the case of the MRAC that (S30) is a nonminimal representation of the MRAC reference model (S26). Therefore, the transfer function obtained from (S30) is

$$h_{mn}^T(sI - A_{mn})^{-1}b_{mn}k^* = k_m \frac{Z_m(s)}{R_m(s)} = W_m(s). \tag{S31}$$

Recalling that $k^* = k_m/k_p$ from the previous section gives

$$h_{mn}^T(sI - A_{mn})^{-1}b_{mn} = k_p \frac{Z_m(s)}{R_m(s)} = \frac{k_p}{k_m}W_m(s). \tag{S32}$$

Using (S21) and (S32), the plant output is

$$y_p(t) = \frac{k_p}{k_m}W_m(s)[\phi^T(t)w(t) + k^* r(t)]. \tag{S33}$$

Subtracting (S28) from (S33) gives

$$e_1(t) = \frac{k_p}{k_m}W_m(s)[\phi^T(t)w(t)] - W_L e_1(t). \tag{S34}$$

Solving (S34), the tracking error dynamics are

$$e_1(t) = k_p W_e(s)[\phi^T(t)w(t)], \tag{S35}$$

where

$$W_e(s) = \frac{Z_m(s)}{R_m(s) + k_L Z_L(s)}. \tag{S36}$$

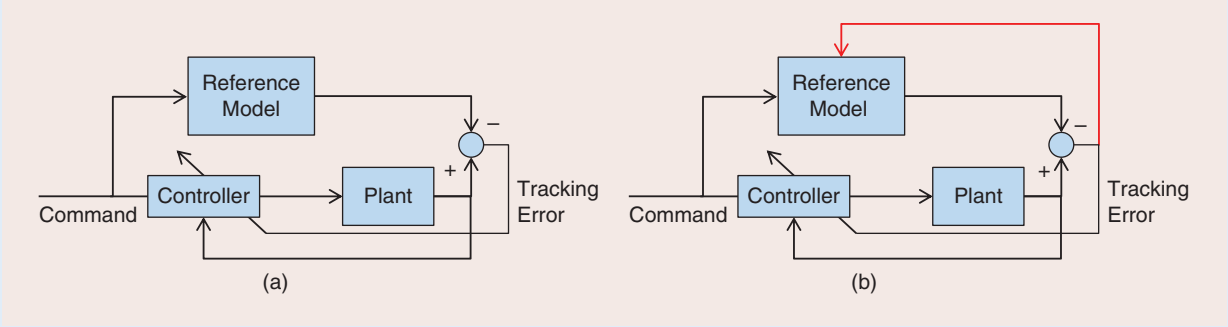

FIGURE S4 (a) Classical model reference adaptive control (MRAC), where controller gains are updated by the tracking error between the plant and reference model outputs. (b) Closed-loop MRAC, where tracking error is also fed back to the reference model to improve the transient response.

Polynomials $k_L Z_L(s)$ and $Z_m(s)$ are of degree $n-1$, while $R_m(s)$ is a monic polynomial of degree n. Therefore, there is enough degrees of freedom such that by choosing a proper L, the transfer function $W_e(s)$ can be realized as an SPR transfer function. It can be shown [S10] that after certain transformations, (S35) can be represented in state-space form similar to (S10) in Lemma 1, and therefore the same MRAC adaptive laws given in (S25) can be employed to force the output tracking error e_1 to converge to zero while keeping all system signals bounded. To summarize, CRM adaptive laws are identical to MRAC adaptive laws. The error feedback used in the reference model dynamics. The designer must be careful about selecting the error feedback gain L such that the resulting transfer function given in (S36) must be SPR.

REFERENCES

[S2] E. Lavretsky, "Reference dynamics modification in adaptive controllers for improved transient performance," in *Proc. American Institute Aeronautics and Astronautics Guidance Navigation and Control Conf.*, 2011, p. 6200.

[S3] N. Harl, K. Rajagopal, and S. Balakrishnan, "Modified state observer for orbit uncertainty estimation," in *Proc. American Institute Aeronautics and Astronautics Guidance Navigation and Control Conf.*, 2011, p. 6616.

[S4] E. Lavretsky, "Adaptive output feedback design using asymptotic properties of LQG/LTR controllers," *IEEE Trans. Autom. Control*, vol. 57, no. 6, pp. 1587–1591, 2012.

[S5] V. Stepanyan and K. Krishnakumar, "MRAC revisited: Guaranteed performance with reference model modification," in *Proc. American Control Conf.*, pp. 93–98, 2010.

[S6] V. Stepanyan and K. Krishnakumar, "M-MRAC for nonlinear systems with bounded disturbances," in *Proc. Conf. Decision and Control*, pp. 5419–5424, 2011.

[S7] T. Yucelen, G. D. L. Torre, and E. N. Johnson, "Improving transient performance of adaptive control architectures using frequency-limited system error dynamics," *Int. J. Control*, vol. 87, no. 11, pp. 2383–2397, 2014. doi: 10.1080/00207179.2014.922702.

[S8] J. Darling, J. Searcy, and S. Balakrishnan, "Modified state observer for atmospheric reentry uncertainty estimation," in *Proc. American Institute Aeronautics and Astronautics Guidance Navigation and Control Conf.*, 2012, p. 4759.

[S9] V. Stepanyan and K. Krishnakumar, "Adaptive control with reference model modification," *J. Guid. Control Dyn.*, vol. 35, no. 4, pp. 1370–1374, 2012.

[S10] T. Gibson, A. Annaswamy, and E. Lavretsky, "Closed-loop reference models for output-feedback adaptive systems," in *Proc. IEEE European Control Conf.*, Zurich, 2013, pp. 365–370.

[S11] T. Gibson, A. Annaswamy, and E. Lavretsky, "Adaptive systems with closed-loop reference models, part I: Transient performance," in *Proc. IEEE American Control Conf.*, Piscataway, NJ, 2013, pp. 3376–3383.

$$\begin{aligned}\dot{x}_p(t) &= A_p x_p(t) + b_p u(t-\tau), \quad y_p(t) = h_p^T x(t),\\ \dot{\omega}_1(t) &= F\omega_1(t) + g u(t-\tau),\\ \dot{\omega}_2(t) &= F\omega_2(t) + g y_p(t),\end{aligned} \tag{19}$$

where $x_p \in \Re^n$ is the original plant state vector, $\omega_1, \omega_2 \in \Re^n$ are newly created additional state vectors, and y_p is the plant output. $A_p \in \Re^{n\times n}$, b_p, and $h_p \in \Re^n$ are the plant state matrix, input vector, and output vector, respectively. $F \in \Re^{n\times n}$ is Hurwitz and $g \in \Re^n$.

Defining the future values of the state variables as $\bar{x}_p(t) \equiv x_p(t+\tau)$, $\bar{y}_p(t) \equiv y_p(t+\tau)$, $\bar{\omega}_1(t) \equiv \omega_1(t+\tau)$ and $\bar{\omega}_2(t) \equiv \omega_2(t+\tau)$, (19) can be rewritten as

$$\begin{aligned}\dot{\bar{x}}_p(t) &= A_p \bar{x}_p(t) + b_p u(t), \quad \bar{y}_p(t) = h_p^T \bar{x}_p(t),\\ \dot{\bar{\omega}}_1(t) &= F\bar{\omega}_1(t) + g u(t),\\ \dot{\bar{\omega}}_2(t) &= F\bar{\omega}_2(t) + g\bar{y}_p(t),\end{aligned} \tag{20}$$

It can be shown that there exist constant controller parameters $\beta_1^* \in \Re^n$, $\beta_2^* \in \Re^n$, and $k^* \in \Re$ such that the controller

$$u(t) = \beta_1^{*T}\bar{\omega}_1(t) + \beta_2^{*T}\bar{\omega}_2(t) + k^* r(t), \tag{21}$$

satisfies the model matching conditions [39]. Observe that this controller is noncasual because it consists of future values of system states, $\bar{\omega}_1(t) \equiv \omega_1(t+\tau)$ and $\bar{\omega}_2(t) \equiv \omega_2(t+\tau)$ that are unavailable at the time of control input $u(t)$ generation. Hence, (21) cannot be realized as is in real applications. However, the unavailable future state values can be predicted using system dynamics, as explained in the following.

It can be shown that the plant output $y_p(t)$ can be expressed as a linear combination of $\omega_1(t), \omega_2(t)$ as

$$y_p(t) = c^T\omega_1(t) + d^T\omega_2(t), \tag{22}$$

where $c, d \in \Re^n$ [51]. Substituting (22) into (19) yields

$$\begin{bmatrix}\dot{\omega}_1(t)\\ \dot{\omega}_2(t)\end{bmatrix} = A\begin{bmatrix}\omega_1(t)\\ \omega_2(t)\end{bmatrix} + b u(t-\tau), \tag{23}$$

where $A \in \Re^{2n\times 2n}$ and $b \in \Re^{2n}$ are given as $A = \begin{bmatrix}F & 0\\ gc^T & F+gd^T\end{bmatrix}$ and $b = \begin{bmatrix}g\\ 0\end{bmatrix}$. Noncasual terms in (21) can then be calculated as

$$\begin{bmatrix}\bar{\omega}_1(t)\\ \bar{\omega}_2(t)\end{bmatrix} = e^{A\tau}\begin{bmatrix}\omega_1(t)\\ \omega_2(t)\end{bmatrix} + \int_{-\tau}^{0} e^{A\eta} b u(t+\eta)\, d\eta. \tag{24}$$

When (24) is substituted into (21), the control signal becomes

$$u(t) = \alpha_1^{*T}\omega_1(t) + \alpha_2^{*T}\omega_2(t) + \int_{-\tau}^{0}\phi^*(\eta)u(t+\eta)\,d\eta + k^* r(t), \tag{25}$$

where $\alpha_i^* = \beta_i^* e^{A\tau}$, $i = 1, 2$ and $\phi^*(\eta) = [\beta_1^{*T}\beta_2^{*T}]e^{-A\eta}$ are the corresponding controller parameters. In this form, the control signal is casual and therefore can be implemented.

In the case of unknown plant parameters, the ideal control parameter values $\alpha_i^*, \beta_i^*, \phi^*(\eta)$, and k^* are unknown. Therefore, the control input $u(t)$ is rewritten as

$$u(t) = \alpha_1^T(t)\omega_1(t) + \alpha_2^T(t)\omega_2(t) + \int_{-\tau}^{0}\phi(\eta,t)u(t+\eta)\,d\eta + k(t)r(t), \tag{26}$$

where the control parameters $\alpha_1(t), \alpha_2(t), \phi(\eta,t)$, and $k(t)$ are adjusted online based on adaptive laws that are discussed below.

Control input (26) can be split into two subsignals as

$$u(t) = u_1(t) + u_2(t), \tag{27}$$

where

$$u_1(t) = \alpha_1^{*T}\omega_1(t) + \alpha_2^{*T}\omega_2(t) + \int_{-\tau}^{0}\phi^*(\eta)u(t+\eta)d\eta + k^*r(t), \tag{28}$$

and

$$u_2(t) = \tilde{\alpha}_1^T(t)\omega_1(t) + \tilde{\alpha}_2^T(t)\omega_2(t) + \int_{-\tau}^{0}\tilde{\phi}(t,\eta)u(t+\eta)d\eta + \tilde{k}(t)r(t), \tag{29}$$

where $\tilde{\alpha}_i(t) = \alpha_i(t) - \alpha_i^*$ for $i = 1,2, \tilde{\phi}(t,\eta) = \phi(t,\eta) - \phi^*(\eta)$, and $\tilde{k}(t) = k(t) - k^*$. The variables $\tilde{\alpha}_i(t)$, $\tilde{\phi}$, and $\tilde{k}(t)$ represent the deviation of the control parameters from their ideal values $\alpha_i^*, \phi^*(\eta)$, and k^*. As explained in (21)–(25), the fixed controller with these ideal values guarantees that the closed-loop transfer function is the same as the reference model transfer function. Therefore, control signal u is the sum of the ideal value of the controller u_1, which is unknown, and the deviation u_2 from the ideal value.

Substituting (27), using (28) and (29), into (19), the closed-loop dynamics are

$$\begin{aligned}\dot{X}_p(t) &= A_{mm}X_p(t) + b_{mm}\Big[\tilde{\theta}(t-\tau)w(t-\tau) + \int_{-\tau}^{0}\tilde{\phi}(t-\tau,\eta)u(t-\tau+\eta)d\eta + k^*r(t-\tau)\Big],\\ y_p(t) &= h_{mm}^T X_p(t),\end{aligned} \tag{30}$$

where

$$\begin{aligned}A_{mm} &= \begin{bmatrix} A_p & b_p\beta_1^* & b_p\beta_2^* \\ 0 & F + g\beta_1^* & g\beta_2^* \\ gh_p^T & 0 & F \end{bmatrix},\\ b_{mm} &= \begin{bmatrix} b_p \\ g \\ 0 \end{bmatrix},\\ h_{mm}^T &= [h_p^T \quad 0 \quad 0],\\ X_p(t) &= [x_p^T(t) \;\; \omega_1^T(t) \;\; \omega_2^T(t)]^T,\\ w(t) &= [\omega_1^T(t) \;\; \omega_2^T(t) \;\; r(t)]^T \text{ and}\\ \tilde{\theta}(t) &= [\tilde{\alpha}_1(t) \;\; \tilde{\alpha}_2(t) \;\; \tilde{k}(t)].\end{aligned}$$

Note that when the deviations of the control parameters from their ideal values are zero, that is $\tilde{(\cdot)} = 0$, the closed-loop dynamics represented by (30) become equivalent to that of the reference model dynamics (18), which show that the system formed by (A_{mm}, b_{mm}, h_{mm}) is a nonminimal representation of the reference model

$$h_{mm}^T(sI - A_{mm})^{-1}b_{mm} \equiv k_p\frac{Z_m(s)}{R_m(s)} = \frac{k_p}{k_m}W_m(s). \tag{31}$$

Using (30) and (31), the plant output is obtained as

$$y_p(t) = \frac{k_p}{k_m}W_m(s)\Big[\tilde{\theta}(t-\tau)w(t-\tau) + \int_{-\tau}^{0}\tilde{\phi}(t-\tau,\eta)u(t-\tau+\eta)d\eta + k^*r(t-\tau)\Big]. \tag{32}$$

Subtracting (16) from (32) yields

$$e_1(t) = \frac{k_p}{k_m}W_m(s)\Big[\tilde{\theta}(t-\tau)w(t-\tau) + \int_{-\tau}^{0}\tilde{\phi}(t-\tau,\eta)u(t-\tau+\eta)d\eta\Big] - W_L e_1(t). \tag{33}$$

Solving (33) for the tracking error e_1 gives

$$e_1(t) = k_p\frac{Z_m(s)}{R_m(s) + k_L Z_L(s)}\Big[\tilde{\theta}(t-\tau)w(t-\tau) + \int_{-\tau}^{0}\tilde{\phi}(t-\tau,\eta)u(t-\tau+\eta)d\eta\Big], \tag{34}$$

where $Z_m(s)/(R_m(s) + k_L Z_L(s)) = W_e(s)$ has sufficient degrees of freedom in terms of the design parameter vector L to be determined as a strictly positive real (SPR) transfer function. The importance of $W_e(s)$ being SPR is explained in "Classical Model Reference Adaptive Control" and "Closed-Loop Model Reference Adaptive Control."

The CRM in (15) can be rewritten as

$$\begin{aligned}\dot{x}_{mm}(t) &= A_{mm}x_{mm}(t) + b_{mm}k^*r(t-\tau) + GL(y_p(t) - y_m(t)),\\ y_m(t) &= h_{mm}^T x_{mm}(t),\end{aligned} \tag{35}$$

where $x_{mm} = [x_p^{*T}(t) \;\; \omega_1^{*T}(t) \;\; \omega_2^{*T}(t)]^T$, $x_p^*(t), \omega_1^*(t)$, and $\omega_2^*(t)$ are the signals in the reference model, corresponding to the signals $x_p(t), \omega_1(t)$, and $\omega_2(t)$ in the closed-loop dynamics, respectively. $G \in \Re^{3n\times n}$ is the constant matrix to transform x_m to the controllable subspace in x_{mm}. The error dynamic $e(t) = X_p(t) - x_{mm}(t)$ (in nonminimal form) is found by subtracting (35) from (30) as

$$\begin{aligned}\dot{e}(t) &= A_e e(t) + b_{mm}\Big[\tilde{\theta}(t-\tau)w(t-\tau) + \int_{-\tau}^{0}\tilde{\phi}(t-\tau,\eta)u(t-\tau+\eta)d\eta\Big],\\ e_1(t) &= h_{mm}^T e(t),\end{aligned} \tag{36}$$

where

$$A_e = A_{mm} - GLh_{mm}^T. \tag{37}$$

It can be shown by the error dynamics (36) that the controller (27)–(29), along with the adaptation laws given as

$$\begin{aligned}\dot{\tilde{\theta}}(t) &= \dot{\theta}(t) = -\operatorname{sgn}(k_p)\Gamma_\theta e_1(t)\omega(t-\tau),\\ \dot{\tilde{\phi}}(t,\eta) &= \dot{\phi}(t) = -\operatorname{sgn}(k_p)\Gamma_\phi e_1(t)u(t-\tau+\eta), \quad -\tau \le \eta \le 0,\end{aligned} \tag{38}$$

stabilize the closed-loop system as long as L is chosen to ensure that $W_e(s)$ is SPR [39]. Furthermore, tracking error $e_1(t)$ converges to zero. $\Gamma_\theta \in \Re^{(2n+1)\times(2n+1)}$ is a diagonal matrix with positive elements and $\Gamma_\phi \in \Re^+$. Γ_θ and Γ_ϕ are free design parameters that are used to adjust the speed of adaptation. In general, the values of these design parameters depend on the application in which the adaptive controller is being utilized. In the following sections, where practical implementation concerns are discussed, a method to choose the adaptation speeds will be presented.

The discussion in this article on the employment of advanced control methodologies should benefit practitioners whose goal is to obtain a fast system response in safety-critical applications where nonlinear dynamics, time-varying parameters, and time delays pose significant challenges.

Note that, in contrast to conventional MRAC, the reference model (15) in the closed-loop MRAC is not bounded a priori, so after showing that the tracking error is bounded, one must ensure that the reference model is indeed bounded. It can be concluded from (15) that this is the case here.

PRACTICAL IMPLEMENTATION ISSUES AND SOLUTIONS

The class of systems that can be controlled by the presented control methodology is not limited to pressure control systems. The theory is very general and can be employed for the control of a wide range of systems with uncertain parameters and time delays. For this reason, practical implementation issues are discussed in this section without specifying any application domain. These issues are not considered during the initial design but arise in real experimental tests. New requirements due to experimental conditions are investigated, and possible solutions are presented. Since the adaptive control approach investigated in this article is comparatively tested against three alternatives [classical MRAC, closed-loop MRAC, and a classical proportional integral (PI) controller], the implementation issues that are relevant for these alternatives are also discussed.

Disturbance Rejection

The goal of the presented closed-loop MRAC (as well as the compared alternative adaptive controllers) is to force the plant output to follow the reference model output while keeping all system signals bounded. However, the disturbances are not explicitly considered. In TDR propulsion systems, the solid propellant in the GG contains metallic particles (see Figure 1), which can cause deposition or ablation at the throat between the GG and ram combuster. The result of this phenomenon is an additive disturbance on the effective throat area. Therefore, the GG pressure controller requires disturbance rejection capabilities. Since the plant model (13) developed for the controller design is first order, the disturbance rejection modification explained below utilizes a scalar plant model.

Consider the plant

$$\dot{y}_p(t) = a_p y_p(t) + b_p(u(t) + d_0), \tag{39}$$

where y_p is the system output, d_0 is the unknown constant disturbance, u is the plant input, and a_p and b_p are the plant parameters. The control signal of the classical MRAC (as well as the closed-loop MRAC) for this scalar plant is

$$u(t) = \theta_0(t) y_p(t) + \theta_r(t) r(t) + \theta_3(t), \tag{40}$$

where θ_0, θ_r, and θ_3 are the adaptive control parameters to be determined, and r is a bounded reference signal. It is noted that if the disturbance term d_0 was not present in (39), then the adaptive control parameter θ_3 would not be needed. The adaptation law for the controller parameters is

$$\dot{\bar{\Theta}}(t) = -\operatorname{sgn}(b_p)\bar{\Gamma} e_1(t)\bar{\Omega}(t), \tag{41}$$

where $\bar{\Theta}^T(t) \equiv [\theta_0(t)\ \theta_r(t)\ \theta_3(t)]$, $\bar{\Omega}^T \equiv [y_p(t)\ r(t)\ 1]$. $\bar{\Gamma}$ is the diagonal adaptation rate matrix (which determines the speed of adaptation), and e_1 is the tracking error given by $e_1 = y_p - y_m$. y_m is the output of the reference model, which is given for the classical MRAC as

$$\dot{y}_m(t) = a_m y_m(t) + b_m r(t). \tag{42}$$

For the closed-loop MRAC, the reference model is determined as

$$\dot{y}_m(t) = a_m y_m(t) + b_m r(t) + l(y_p(t) - y_m(t)). \tag{43}$$

For the reference models given in (42) and (43), $a_m \in \Re^-$ and $b_m \in \Re^+$. To make the reference model output y_m follow the reference input r, a_m is selected such that $a_m = -b_m$. The reference model feedback gain l in (43) is selected as a real positive number, which satisfies the stability conditions explained in "Classical Model Reference Adaptive Control" and "Closed-Loop Model Reference Adaptive Control."

For the DR-CRM adaptive controller, the control signal is

$$u(t) = \alpha_y(t) y_p(t) + \int_{-\tau}^{0} \lambda(t,\eta) u(t+\eta)\, d\eta + k(t) r(t) + \theta_3(t). \tag{44}$$

As before, the control term θ_3 would not be needed if the plant (39) did not have the disturbance d_0. The adaptive laws for the controller parameters α_y, λ, k, and $\theta_3 \in \Re$ are

$$\begin{aligned} \dot{\theta}(t) &= -\operatorname{sgn}(b_p)\Gamma_\theta e_1(t)\omega(t-\tau), \\ \frac{\partial \lambda}{\partial t}(t,\eta) &= -\operatorname{sgn}(b_p)\gamma_\lambda e_1(t) u(t+\eta-\tau) \quad -\tau \le \eta \le 0, \end{aligned} \tag{45}$$

where $\theta^T(t) \equiv [\alpha_y(t)\ k(t)\ \theta_3(t)]$ and $\omega^T(t) \equiv [y_p(t)\ r(t)\ 1]$. Γ_θ and γ_λ are the adaptation rates. e_1 is the tracking error, which is calculated as $e_1 = y_p - y_m$, where y_m is the output of the CRM, whose dynamics are governed by

$$\dot{y}_m(t) = a_m y_m(t) + b_m r(t-\tau) + l(y_p(t) - y_m(t)), \tag{46}$$

where $a_m \in \Re^-$ and $b_m \in \Re^+$. Similarly, to make the reference model output y_m follow the reference input r, a_m is selected such that $a_m = -b_m$. The CRM feedback gain l is selected as a positive real number to ensure stability conditions.

Robustness

The design of the delay resistant closed-loop reference model adaptive controller is an idealized case, where the delay-free part of the plant dynamics is assumed to be linear and time invariant with unknown but constant parameters. Furthermore, the measurements are assumed to be perfect. However, in reality, no plant is truly linear or finite dimensional. Parameters may vary with time and operating conditions, and measurements are always contaminated with noise. The plant model used for the controller design is always an approximation of reality. Adaptation of the control parameters (45) is accomplished by the tracking error e_1. Therefore, without any regard for the source of this error, the adaptive parameters will continue to adapt to compensate for it. However, adaptation to compensate for the error that is caused by nonideal conditions is undesirable since it is known to cause the parameters to drift instead of converging to a certain region. This may cause the closed-loop system to eventually enter an unstable regime. A robustfying modification against possible parameter drifts in adaptive controller parameters is needed. One common remedy to prevent parameter drift is the projection algorithm [52].

Consider a classical MRAC law, such as the one given in (41): $\dot{\Theta}(t) = -\operatorname{sgn}(b_p) e_1(t) \Omega(t)$. Overbars on the parameters are removed for simplicity. For generality, assume that the control parameter vector has k elements $\Theta(t)$, and therefore $e_1 \in \Re$ and $\Omega \in \Re^k$. The adaptation rate matrix $\Gamma \in \Re^{k\times k}$ is removed from the adaptation law and used in the Γ-Projection, which is presented next. As discussed previously, this adaptive law will cause parameter drift in the presence of nonideal conditions. However, when the projection algorithm is implemented, the norm is always kept inside a ball, such that $\|\Theta\| \le \Theta_{\max}(\sqrt{1+\epsilon})$, where $\Theta_{\max}$ is a threshold to trigger the algorithm and ϵ is the projection tolerance. This is achieved by modifying the above adaptive law as

$$\dot{\Theta} = \operatorname{Proj}_\Gamma(\Theta, -\operatorname{sgn}(b_p) e_1 \Omega), \tag{47}$$

where the Γ-Projection operator $\operatorname{Proj}_\Gamma$ is defined as

$$\operatorname{Proj}_\Gamma(\Theta, y) \triangleq \begin{cases} \Gamma y - \Gamma \dfrac{\nabla f(\Theta)(\nabla f(\Theta))^T}{(\nabla f(\Theta))^T \Gamma \nabla f(\Theta)} \Gamma y f(\Theta), \\ \qquad \text{if } \|\Theta\| > \Theta_{\max} \text{ and } y^T \Gamma \nabla f(\Theta) > 0 \\ \Gamma y, \qquad \text{otherwise} \end{cases} \tag{48}$$

where $y \in \Re^k$. $\nabla f(\Theta) \in \Re^k$ is the gradient vector of a differentiable convex function $f : \Re^k \to \Re$, which is defined as

$$f(\Theta) = \frac{\|\Theta\|^2 - \Theta_{\max}^2}{\epsilon \Theta_{\max}^2}. \tag{49}$$

Note that, when the projection operator (48) is used in (47), the variable y corresponds to the unmodified adaptive law.

Equations (47)–(49) describe the following adaptation procedure: If the norm of the controller parameter vector $\|\Theta\|$ is smaller than a given threshold $\Theta_{\max}$, then the adaptive law $\dot{\Theta} = -\Gamma \operatorname{sgn}(b_p) e_1 \Omega$ is implemented without any modification. However, if the norm is larger than this threshold and keeps growing, then the projection algorithm is triggered and the adaptive law is modified as

$$\dot{\Theta} = -\Gamma \operatorname{sgn}(k_p) e_1 \Omega - \Gamma \frac{\nabla f(\Theta)(\nabla f(\Theta))^T}{(\nabla f(\Theta))^T \Gamma \nabla f(\Theta)} \times (-\Gamma \operatorname{sgn}(b_p) e_1 \Omega) f(\Theta). \tag{50}$$

It is shown in [52] that this approach prevents the parameter drift and keeps the control parameter vector norm within a specified bound, such that $\|\Theta\| \le \Theta_{\max}(\sqrt{1+\epsilon})$.

Although the effect of the projection algorithm to prevent parameter drift is observed in the experiments, no well-defined procedure exists to determine the upper bound $\Theta_{\max}$ on the controller parameter vector Θ. One method is to calculate this bound using the worst-case uncertainty. Another method is to conduct several experiments without projection and observe the variation of controller parameters, which help define a reasonable upper bound. A third approach is setting the initial values for the controller parameters that would satisfy the matching conditions for the nominal plant dynamics and then determining the upper bound for the parameters as a certain percentage higher than these initial values. The second method is employed during the experiments presented in this article.

Digital Implementation

The DR-CRM adaptive controller (and the alternatives considered here) are written in the continuous-time domain. However, the computer implementations must be written in discrete time. This is typically not an issue and can be addressed using conventional discretization methods such as Euler's method. However, extra care must be taken for the integral term in the DR-CRM input (44) since the discretization also affects the corresponding adaptive law. The integral term is approximated as

$$\int_{-\tau}^{0} \lambda(t,\eta) u(t+\eta)\, d\eta = \sum_{i=1}^{m} \lambda_i(t) u(t - i dt) = \bar{\lambda}^T(t) \bar{u}(t), \tag{51}$$

where $dt = 50$ ms is the sampling interval used for the experiments, $\tau = 300$ ms is the time delay, and the number of samples created during τ seconds is $m = \tau/dt = 6$. $\bar{\lambda} \in \Re^m$ is the vector containing parameters $\bar{\lambda}^T(t) = [\lambda_1(t) \ldots \lambda_m(t)]$

The presented solution, termed the delay-resistant closed-loop reference model adaptive controller is investigated through simulations and experimental studies, where comparisons with progressively more sophisticated control approaches are carefully conducted.

and $\bar{u} \in \Re^m$ is the delayed input vector $\bar{u}^T(t) = [u(t-dt) \ldots u(t-mdt)]$. Accordingly, the adaptation law (45) is updated as

$$\dot{\bar{\theta}}(t) = -\operatorname{sgn}(b_p)\bar{\Gamma}_{\bar{\theta}}\, e_1(t)\,\bar{\omega}(t), \tag{52}$$

where

$$\bar{\theta}(t) = \begin{bmatrix} \alpha_y(t) \\ \lambda_1(t) \\ \vdots \\ \lambda_m(t) \\ k(t) \\ \theta_3(t) \end{bmatrix}, \quad \bar{\omega}(t) = \begin{bmatrix} y_p(t) \\ u(t-dt) \\ \vdots \\ u(t-mdt) \\ r(t) \\ 1 \end{bmatrix}. \tag{53}$$

In some applications where the time delay in the system varies depending on the operating condition, the number of samples m also becomes variable. This may create jumps in the control signal. There are ways to address this phenomenon, but they are out of the scope of this article. See [34] for a more detailed discussion.

Initialization of the Controller Parameters

There are several ways to initialize the adaptive control parameters. In some applications, the designer may choose to set these values to zero and let the adaptive control parameters "learn by experience" by updating their values based on their adaptive laws. Another approach is to inject preexisting knowledge about the plant dynamics into the control parameters. This is achieved by picking the initial parameter values that would satisfy the model matching conditions for the nominal plant dynamics. Here, the nominal plant dynamics are the part of the dynamics that are known by the designer. For example, the designer might know that the mass of the system is nominally m kg. However, due to various uncertainty sources, the mass of the system can be different from the nominal value in real operation. Using the nominal plant dynamics and fixed version of the adaptive controller (which is simply the same control signal with constant control parameters), the nominal closed-loop transfer function can be determined. By equating this transfer function to that of the reference model, the nominal ideal values of the control parameters can be determined. When the initial values of the adaptive control parameters are set to these values, the knowledge of the nominal plant dynamics is introduced to the adaptive controller.

For a plant with time delays, the classical MRAC or the CRM adaptive controller cannot provide model-matching conditions since they do not contain any delay-compensating term. For these controllers, the nominal ideal values are found using the delay-free part of the nominal plant dynamics. Since these values are not truly ideal, additional tuning might be necessary to obtain the best performance in the experiments. For the experiments presented here, $\theta_0(0)$ and $\theta_r(0)$ in (40) had to be lowered from their calculated values. On the other hand, the initial parameters for the DR-CRM adaptive controller are set to satisfy the exact nominal model matching conditions. The initial parameter $\theta_3(0)$ is set to zero for all adaptive controllers.

Setting the Adaptation Speed

Setting the speed of adaptation is one of the hardest issues in adaptive control implementations. The speed is commonly set using experience or trial and error. Another method assumes that the control parameters eventually reach their ideal values and then force the parameters to reach these values within three time constants. Considering a generic adaptive law $\dot{\Theta} = -\Gamma e_1 \Omega$, where Γ is the adaptation rate matrix, e_1 is the tracking error, and Ω is the vector of corresponding system signals. Assuming that e_1 and elements of Ω are the same order of magnitude as the reference signal r, the adaptation speed for a particular parameter θ_i is chosen as

$$\Gamma_{ii} = \frac{|\,\theta_i^*\,|}{3\tau_m(\bar{r})^2}, \tag{54}$$

where θ_i^* is the ideal value of the ith controller parameter, τ_m is the smallest time constant of the reference model, and $\bar{r}$ is the maximum possible amplitude of the reference signal [53]. Since the ideal controller parameters θ_i^* are unknown, the nominal ideal values (calculated using the nominal plant dynamics) are used instead.

Adaptation rates obtained from (54) are calculated for the worst-case scenario, which is usually valid at the beginning of the operation when the tracking error and system states are of the same order of magnitude as the reference

signal. Moreover, (54) requires the estimation of the ideal control parameters. Due to these approximations, a matrix W to fine-tune the adaptation rates as $\Gamma_W = \Gamma W$ is introduced where

$$W = \begin{bmatrix} p_1 & 0 & 0 \\ 0 & p_2 & 0 \\ 0 & 0 & p_3 \end{bmatrix}, \tag{55}$$

and adjustable constants $p_{1,2,3}$ are used for the fine-tuning process.

Determining the Feedback Gain l of the Reference Model

The feedback term $l(y_p(t) - y_m(t))$ used in the CRMs (43) and (46) helps suppress the oscillations in the case of high adaptation rates. Although this advantage is demonstrated both in simulations and experiments, it is known that an undesired effect known as peak phenomena can be observed if care is not taken when choosing the gain l used in this term [54]. The peak phenomena is the undesired increase of reference model output initially observed when a high gain in the feedback term is selected. Therefore, a procedure is needed to determine the optimum value of this gain, which may help reduce the time and effort spent tuning the controller. Such a procedure, inspired by [41], is defined as follows:

1) Determine the adaptation rates using (54).
2) Place the adaptation rates of all parameters into a vector, $\bar{\gamma}$, and determine its norm, $\|\bar{\gamma}\|$.
3) Choose the closed-loop reference feedback gain as $l = \|\bar{\gamma}\|$.
4) Increase/decrease l and $\bar{\gamma}$ together by maintaining $l = \|\bar{\gamma}\|$ until a desired tracking performance is obtained.

Controller Design Procedure

A detailed procedure for facilitating the adaptive controller design is defined as follows:

1) Determine the reference model dynamics by choosing appropriate (A_m, b_m, h_m) for the performance specifications of the closed-loop system.
2) The signals $\omega_{1,2}(t)$ in (19) are generated by choosing a controllable pair (F, g). Since these signals operate like state observers, the eigenvalues of F should be faster than the reference model dynamics. Note that if the plant is first order, these signals are not required.
3) Set the initial conditions of the controller parameters using the method explained in the section "Initialization of the Controller Parameters."
4) Determine the adaptation rates, as explained in the section "Setting the Adaptation Speed."
5) Adjust the model reference feedback gain l using the procedure explained in the section "Determining the Feedback Gain l of the Reference Model."
6) Integrate the projection algorithm provided in (47) to the adaptation laws.

Recall that the above procedure streamlines the design and minimizes the tuning effort. Depending on the application, additional tuning may be necessary.

The adaptive controllers implemented in this article require minimal amounts of computational resources and memory. For example, the DR-CRM adaptive controller (having the highest number of terms in the controller signal) needs only 256 B of memory for data storage. It has 116 operations per cycle, which corresponds to approximately 2320 floating-point operations per second. "Memory Requirement and Computational Load for the Delay-Resistant Closed-Loop Reference Model Adaptive Controller" gives the detailed memory requirement and computational load calculations.

Memory Requirement and Computational Load for the Delay-Resistant Closed-Loop Reference Model Adaptive Controller

There is a limited amount of computational space dedicated to the pressure controller in the main flight computer of the throttleable ducted rocket. Therefore, it is desired to determine the computational burden of the delay-resistant closed-loop reference model adaptive controller to determine if it satisfies the constraints as the pressure controller.

The input time delay is 300 ms on average, whereas the sampling interval of the controller cycle is 50 ms, which adds six controller parameters λ_i and six states $u(t - mdt)$ to the controller structure [see (51)]. There are nine states, nine controller parameters, and nine multiplication results in the controller signal (44). Nine terms are allocated as the calculation results of the adaptive laws (45). In adaptation laws, there are four terms to define the reference model (a_m, b_m, ℓ, and y_m), one tracking error term and nine adaptation rate terms. In addition, there are 13 terms in the projection algorithm ($\Theta_{\max}, \epsilon, \|\Theta\|, f$, and ∇f). Overall, there are 64 single-precision float variables, which need 256 B of memory space.

A total of nine multiplication and eight summation operations are needed to define the controller signal. There exist 18 multiplications in the adaptive law calculations, and nine summation operations are required to update the controller parameters. In addition, four summation and three multiplication operations are needed to form the reference model output and tracking error. Furthermore, in the projection algorithm, there are two comparisons and one logical operation, and 18 summation and 43 multiplication operations, along with a square root operator. In total, 116 floating-point operations are conducted per controller cycle, which runs with a sampling rate of 50 ms, resulting in 2320 floating-point operations per second.

The goal of the presented closed-loop MRAC (as well as the compared alternative adaptive controllers) is to force the plant output to follow the reference model output while keeping all system signals bounded.

IMPLEMENTATION OF THE CONTROLLER: SIMULATIONS AND EXPERIMENTS

The DR-CRM adaptive control approach in this article combines adaptive delay compensation and adaptive transient improvement and can therefore be employed to control any system that can be represented using linear differential equations (or that can be linearized with reasonable accuracy around operating points), with uncertain parameters. The pressure control problem is one of the systems that fits into this category. In this section, realization of the controller responsible for the pressure of a cold-air test setup is presented using both numerical simulations and experimental studies. In these demonstrations, the controller is carefully compared with alternative adaptive controllers. Selected alternative controllers are the classical MRAC and CRM adaptive control. All of the evaluated adaptive controllers are designed and tuned using the procedures presented in the section "Practical Implementation Issues and Solutions." In addition to the adaptive alternatives, a fixed PI is also evaluated for the pressure control task. The PI controller, with transfer function

$$G_{PI}(s) = K_p\left(1 + \frac{1}{T_i s}\right), \tag{56}$$

is designed using the plant dynamics in (13). Since the goal in adaptive control designs is to make the controller follow the reference model output, closed-loop performance specifications in these systems are imposed using reference models. Similarly, scalar PI controller parameters K_p and T_i are selected to make the closed-loop dynamics provide a similar response to the reference model (42). Frequency response plots of the reference model and the PI-compensated closed-loop system are provided in Figure 9, which shows considerable agreement.

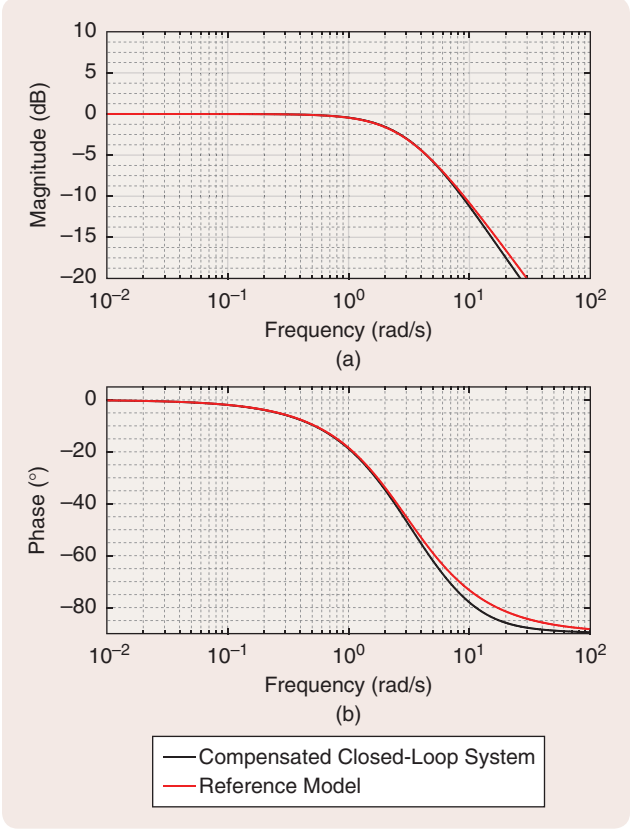

FIGURE 9 A comparison of the Bode plots of the reference model and compensated closed-loop system with the proportional-integral (PI) controller. The gains of the PI controller are selected such that the compensated closed-loop system has a similar frequency response up to the bandwidth frequency (corresponds to the maximum frequency where the gain response drops by 3 dB).

Numerical Simulations

The full nonlinear model of the cold-air test setup, which is presented in the section "Building the Nonlinear Model Through First Principles and Data," is used for the simulations. The reference model used for the design of adaptive controllers is chosen to satisfy the performance specifications listed in Table 1.

The performance of MRAC is first compared with the PI controller to demonstrate the advantage of adaptation when the operating point changes. Next, three adaptive controllers (MRAC, CRM adaptive control, and DR-CRM adaptive control) are compared to present the advantages of transient improvement and delay compensation methods. In these adaptive control comparisons, demanding tracking tasks are utilized to reveal the performance differences between the controllers. Numerical simulations are conducted using Matlab with a sampling interval of 50 ms.

TABLE 1 The specifications of the chosen reference model, which are tailored based on the performance requirements of the pressure loop response.

Steady-State Error	Rise Time	Settling Time (5%)	Maximum Overshoot
0 %	0.6 s	1.5 s	10%

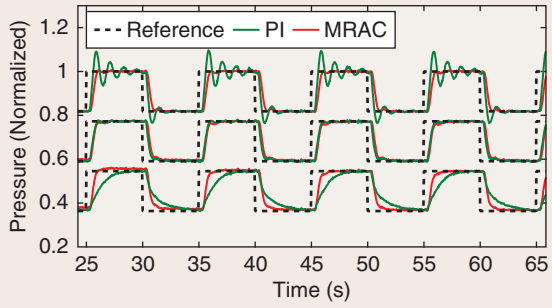

FIGURE 10 The tracking curves for the proportional-integral (PI) controller and model reference adaptive control (MRAC) at three different operating points in the simulations. Although the PI controller and MRAC show very similar performances around the normalized nominal pressure (between 0.6 and 0.8), the PI controller presents an oscillatory response for higher pressures and a slow response for lower pressures. Alternately, MRAC provides a more consistent performance across operating points.

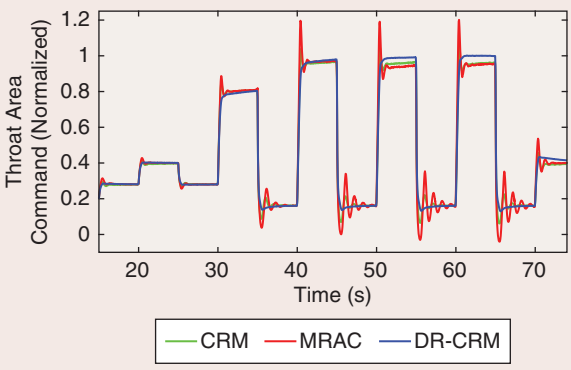

FIGURE 12 The evolution of control inputs of model reference adaptive control (MRAC), closed-loop reference model (CRM) adaptive control, and delay-resistant closed-loop reference model (DR-CRM) adaptive control in simulations. The DR-CRM controller provides the smoothest control input.

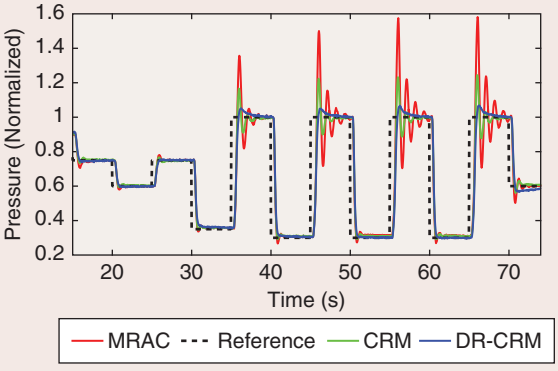

FIGURE 11 Reference tracking of model reference adaptive control (MRAC), closed-loop reference model (CRM) adaptive control, and delay-resistant closed-loop reference model (DR-CRM) adaptive control in simulations. The MRAC, CRM adaptive controller, and DR-CRM adaptive controller provide similar performances for small variations in the pressure demand. However, the MRAC response becomes oscillatory once the demanded variation is increased threefold. Although the CRM adaptive controller provides a considerably more damped response compared to the MRAC, the best response is obtained for the case where the DR-CRM adaptive controller is employed.

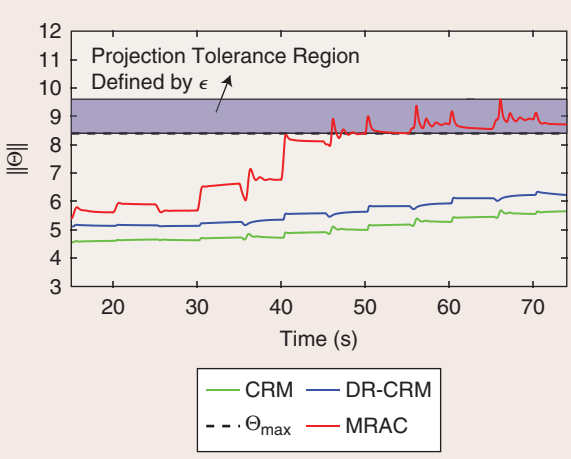

FIGURE 13 Controller parameters of model reference adaptive control (MRAC), closed-loop reference model (CRM) adaptive control, and delay-resistant closed-loop reference model (DR-CRM) adaptive control in simulations with the projection boundary. MRAC parameters reach the projection boundary and stay within the projection tolerance limits.

Model Reference Adaptive Control Versus the Proportional Integral Controller

In Figure 10, the simulation results demonstrate the performance of the MRAC and the PI controller. Note that although the PI controller and MRAC show very similar performances around the normalized nominal pressure (between 0.6 and 0.8), the closed-loop system with the PI controller presents an oscillatory response for higher-pressure operating conditions and a slow response for lower pressures. In contrast, the MRAC can adapt to changing operating conditions and provides a more consistent performance across operating points.

Comparative Evaluation of Adaptive Controllers

The promise of CRM and delay compensation modifications for the conventional MRAC controller is that they provide higher performance without causing excessive oscillations. To demonstrate the impact of these modifications, more demanding reference trajectories than those presented in Figure 10 are used for the reference tracking tests. In addition, time constant of the reference model τ_m is halved to obtain a fast response. The results of these simulations are given in Figures 11–13.

The MRAC, CRM adaptive controller, and DR-CRM adaptive controller provide similar performances for small variations in the pressure demand. However, the MRAC

response becomes oscillatory once the demanded variation is increased threefold. Although the CRM adaptive controller provides a considerably more damped response compared to MRAC, the best response is obtained when the DR-CRM adaptive controller is employed. Figure 12 shows that the DR-CRM controller provides the smoothest control input. In Figure 13, adaptive control parameters are shown where MRAC parameters hit the projection boundary and stays within the projection tolerance limits.

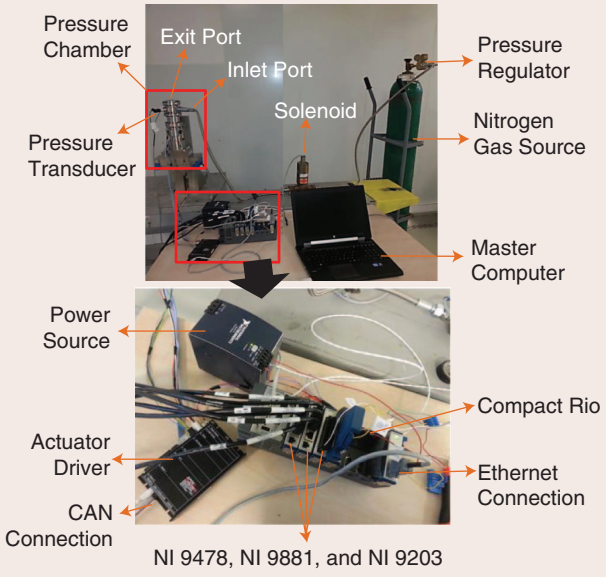

FIGURE 14 A cold-air test setup. The inlet port of the pressure chamber is connected to a nitrogen gas source of 230 bars through a pressure regulator. A solenoid is located between the pressure chamber and the pressure regulator. The effective throat area at the outlet port of the pressure chamber is altered by the actuator and valve mechanism. The output shaft of the motor is connected to a gear box and a ball screw spindle. The other side of the spindle is connected to a conical pintle (see Figure 5). A pressure transducer is located inside the pressure chamber.

Experimental Studies

The experimental results are obtained using a cold-air test setup, which is designed and manufactured by Roketsan, Inc. Figure 4 shows a schematic of the overall system, and Figure 14 is the real experimental system. The pressure chamber has two ports: inlet and exit. The inlet port is connected to a nitrogen gas source of 230 bars through a pressure regulator. The pressure regulator ensures safe test conditions by adjusting the inflow pressure. There is a solenoid between the pressure chamber and the pressure regulator to stop the flow in case of emergencies. The outlet port of the pressure chamber has the shape of a nozzle whose effective throat area is continuously altered during the operation by the actuator and valve mechanism. An EC-max 30, 60-W, 24-V brushless dc motor (Maxon Motor Company) with an EPOS2 70/10 driver is used as the actuator. The output shaft of the motor is connected to a gear box and a ball screw spindle. The other side of the spindle is connected to a conical pintle, which is located such that its linear position determines the effective throat area at the outlet of the pressure chamber (see Figure 5). A pressure transducer is located inside the pressure chamber, which provides real-time pressure data to the controller. A slave Compact Rio computer (National Instrument) running Labview software collects data from the pressure transducer, runs the pressure controller cycles to calculate the necessary effective throat area, and sends this data to the actuator driver that is responsible for controlling

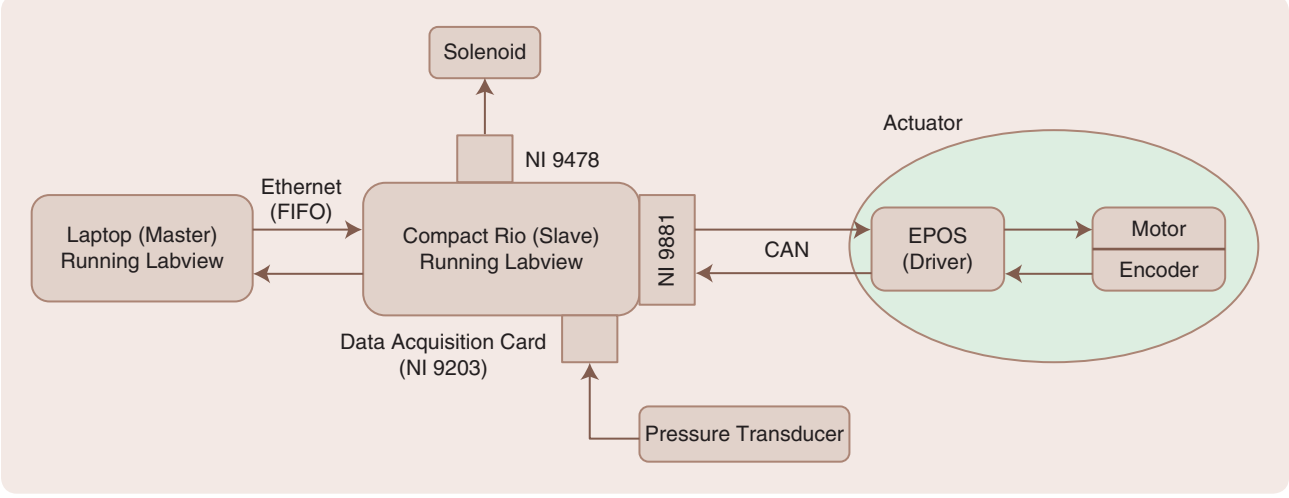

FIGURE 15 A schematic of the cold-air test setup hardware and data communication. A slave Compact Rio computer is used to collect data from the pressure transducer, run the pressure controller cycles, and send data to the actuator driver. The communication between Compact Rio and the actuator driver card is via the NI 9881 card using a controller area network (CAN) bus protocol. The pressure transducer is connected to the data acquisition card (NI 9203) that is also connected to the Compact Rio. Communication between the master and slave computers is realized via Ethernet using a first-in, first-out methodology. The solenoid is controlled by the master computer via the NI 9478 digital card.

the actuator position. The communication between the slave Compact Rio computer and the actuator driver card is through an NI 9881 card using a controller area network bus protocol. Pressure transducer is connected to the data acquisition card (NI 9203) that is also connected to the Compact Rio. All of the algorithms for data acquisition, pressure controller calculations, data sending, and corresponding communication phases are prepared in the master computer prior to the experiments using Labview, and the code is embedded to the slave Compact Rio computer through an Ethernet connection. The master computer monitors the experiment in real time and is able to intervene in the experimental process in case of a safety hazard. The solenoid located in between the pressure chamber and pressure regulator is controlled by the master computer through the NI 9478 digital card. A detailed schematic of the hardware and data communication is given in Figure 15.

The same scenarios used for the simulations are employed for the experimental tests. First, better performance of MRAC over the PI controller is demonstrated by performing experiments at three different operation points with the same controller gains and parameters used in the simulations. A comparative evaluation showing the advantage of the DR-CRM adaptive controller over other adaptive controllers is then presented. Finally, an experiment is conducted for a larger period of time to show the effectiveness of the projection algorithm. All of the numbers in the figures are normalized. The adaptation rates used for these experiments are the same as those used in the simulations.

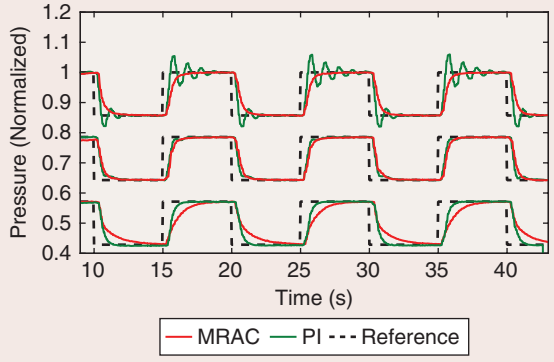

FIGURE 16 Test results of the proportional-integral (PI) controller and model reference adaptive control (MRAC) for three different operating conditions. The PI controller shows acceptable performance at the nominal operating point. However, as the operating point deviates from the nominal design conditions, MRAC provides consistent transient performance.

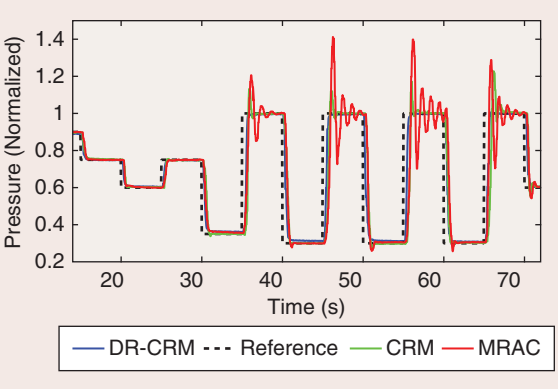

FIGURE 17 Reference tracking of model reference adaptive control (MRAC), closed-loop reference model (CRM) adaptive control, and delay-resistant closed-loop reference model (DR-CRM) adaptive control in experiments. The DR-CRM adaptive controller manages the demanding operation conditions in the experiments (the time constant of the reference model τ_m is halved) and provides a reasonable performance.

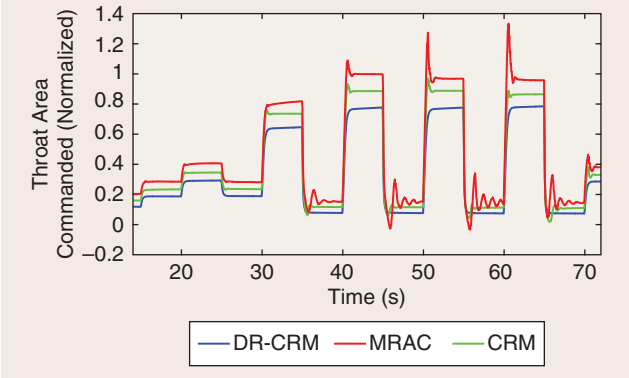

FIGURE 18 The evolution of control inputs of model reference adaptive control (MRAC), closed-loop reference model (CRM) adaptive control, and delay-resistant closed-loop reference model (DR-CRM) adaptive control in experiments. The DR-CRM adaptive controller has the smoothest controller input.

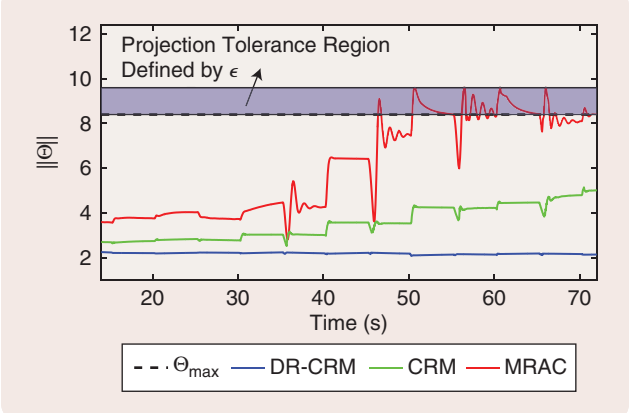

FIGURE 19 Controller parameters of model reference adaptive control (MRAC), closed-loop reference model (CRM) adaptive control, and delay-resistant closed-loop reference model (DR-CRM) adaptive control in experiments. The controller parameters of MRAC reach the projection boundary but are then prevented from further growth.

For a plant with time delays, the classical MRAC or the CRM adaptive controller cannot provide model-matching conditions since they do not contain any delay-compensating term.

Model Reference Adaptive Control Versus the Proportional Integral Controller

The test results are given in Figure 16. The PI controller shows an acceptable performance at the nominal operating point, the linearized model of which was used for the controller design. However, as the operating point deviates from the nominal design conditions, the advantage of the adaptive controller (which provides consistent transient performance at different operating conditions) is observed.

Comparative Evaluation of Adaptive Controllers

To demonstrate the performance differences between the adaptive controllers, a more challenging reference signal is used and the time constant of the reference model τ_m is halved. The same controller design parameters are used as in the simulations.

Experiment results are given in Figures 17–19. The results exhibit similar trends with the simulations, with the CRM and DR-CRM adaptive controller having slightly more damped responses. The DR-CRM adaptive controller is able to address the demanding operation conditions in the experiments and provides a reasonable performance. The CRM adaptive controller (damping most of the oscillations as intended) results in undesirable high amplitude overshoots. The MRAC's response is similar to that of the other two adaptive controllers for small pressure deviation demands but becomes oscillatory for larger deviations in the reference signal. The DR-CRM adaptive controller has the smoothest controller input, as shown in Figure 18. Figure 19 shows that controller parameters of MRAC hit the projection boundary, but are then prevented to grow further.

The effect of the projection algorithm can be observed in the experiments that are conducted for longer times. Figure 20 presents the evolution of the norm of the MRAC controller parameters in a longer test whose tracking curve is depicted in Figure 21. The controller parameters tend to increase due to nonideal situations such as unmodeled dynamics, disturbances, and noise. However, the projection algorithm keeps them within a predefined bound. The milder reference model (the same as the PI controller comparison) is used in this experiment.

SUMMARY AND FUTURE WORK

Uncertainties, time delays, and the safety-critical nature of the pressure control systems (especially those that require very high operating pressures) pose a significant challenge for the control system designer. The general approach in the control design of these types of critical systems compromises performance to eliminate undesired transients. The results presented here show that combining the right complementary control tools can make dramatic performance improvements in these complex control problems without causing dangerous oscillations. Specifically, it is demonstrated that merging three main control themes (delay compensation, adaptation, and transient performance improvement) using error feedback in reference models to obtain a fast and well-damped system response in uncertain time-delay systems. The DR-CRM adaptive controller combines these features. Numerical simulations and

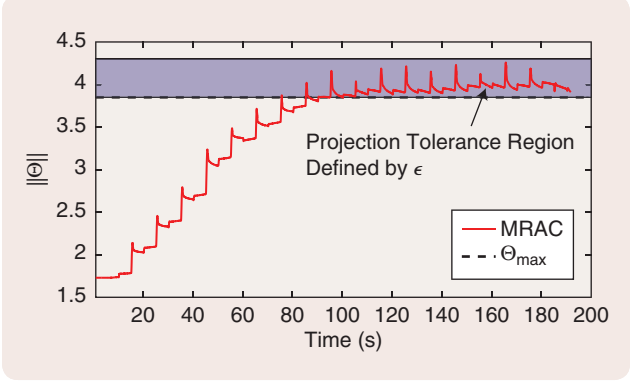

FIGURE 20 The norm of the model reference adaptive control (MRAC) parameters in a long-term test. The controller parameters tend to increase, but the projection algorithm maintains them within a predefined bound.

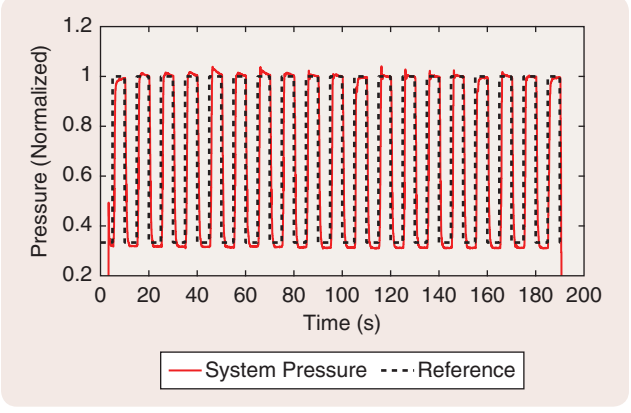

FIGURE 21 Pressure tracking in the long-term test. Stable tracking is achieved for long time periods due to the projection algorithm keeping the controller parameters bounded.

The investigated DR-CRM adaptive controller presents an opportunity to significantly improve the closed-loop performance of the class of systems that are safety critical and contain parameter uncertainties and large time delays.

experimental studies are presented, where the controller manages the pressure of a cold-air test setup, which is considered to be a validation platform for the development of TDRs. A detailed nonlinear mathematical model of the test setup is presented. Solutions to address practical implementation issues are suggested to ensure the robustness of the controller against nonideal experimental conditions. These issues are not reserved for the pressure control problem but are encountered in almost all adaptive control implementations. A detailed control design guide is also provided for researchers and practitioners who are familiar with basic control theory.

The DR-CRM controller is compared to a classical MRAC, CRM adaptive control, and PI controller. The simulations and experiments show that MRAC has advantages over a constant gain PI controller. Furthermore, more demanding conditions reveal the advantage of the DR-CRM adaptive controller over the CRM adaptive controller and MRAC. The promise of the projection algorithm to prevent the drift of the adaptive control parameters is also validated both in simulations and experiments.

The investigated DR-CRM adaptive controller presents an opportunity to significantly improve the closed-loop performance of the class of systems that are safety critical and contain parameter uncertainties and large time delays. Future challenges to enlarge the class of real-life systems that benefit from high-speed and safe control include time-varying dynamics with fast-changing parameters and time-delays, actuators with limited authority, and the need for discrete time-domain design due to nonideal sampling.

AUTHOR INFORMATION

Anil Alan is a Ph.D. student at Middle East Technical University, Turkey. He is currently a motion systems expert design engineer for Aselsan, Inc. He received the B.S. degree in mechanical engineering from Middle East Technical University and the M.S. degree in mechanical engineering from Bilkent University, Ankara, Turkey, in 2013 and 2017, respectively. His research interests are dynamic system modeling and robust adaptive control.

Yildiray Yildiz (yyildiz@bilkent.edu.tr) is an assistant professor and director of the Systems Lab at Bilkent University, Ankara, Turkey. He received the B.S. degree (valedictorian) in mechanical engineering from the Middle East Technical University, Ankara, Turkey, in 2002; the M.S. degree in mechatronics engineering from Sabanci University, Istanbul, Turkey, in 2004; and the Ph.D. degree in mechanical engineering with a mathematics minor from the Massachusetts Institute of Technology, Cambridge, in 2009. He held postdoctoral associate and associate scientist positions with NASA Ames Research Center, Mountain View, California, from 2009 to 2010, and he was employed by the University of California, Santa Cruz, through its University Affiliated Research Center from 2010 to 2014. He is the recipient of the ASME Best Student Paper in Conference award (2008), the NASA Group Achievement Award (2012) for outstanding technology development of the CAPIO system at the Vertical Motion Simulator supporting NASA's Green Aviation Initiative, and the Turkish Science Academy's Young Scientist Award (2017). He was a member of the AIAA Guidance, Navigation, and Control Technical Committee from 2010 to 2013. He has been an IEEE Conference Editorial Board associate editor since 2015 and an associate editor for *IEEE Control Systems Magazine* since 2016. His research interests include adaptive control, time-delay systems, applications of game theory, applications of reinforcement learning, automotive control, and aerospace control. He can be contacted at Bilkent University, Mechanical Engineering Department, 06800, Bilkent, Ankara, Turkey.

Umit Poyraz is a propulsion system senior design engineer at Roketsan, Inc., where he has been since 2011. He received the B.S. degree in mechanical engineering from TOBB University of Technology, Ankara, Turkey, in 2009 and the M.Eng. degree in mechanical engineering from Esslingen University of Applied Sciences, Stuttgart, Germany, in 2011. He is currently a Ph.D. student in the Aerospace Engineering Department at Middle East Technical University, Ankara, Turkey. His research interests are high-speed propulsion and test technologies and supersonic and hypersonic wind tunnels.

REFERENCES

[1] H.-L. Besser and G. Kurth, "Meteor: European air dominance missile powered by high energy throttleable ducted rocket," in *Proc. RTO-MP-AVT-208*, 2012, pp. 1–17.

[2] S. Burroughs, "Status of army Pintle technology for controllable thrust propulsion," in *Proc. 37th AIAA/ASME/SAE/ASEE Joint Propulsion Conf. and Exhibit*, Salt Lake City, UT, 2001.

[3] C. Bauer, F. Davenne, N. Hopfe, and G. Kurthy, "Modeling of a throttleable ducted rocket propulsion system," in *Proc. AIAA/ASME/ASEE Joint Propulsion Conf. and Exhibit*, San Diego, CA, 2011.

[4] K. Xie, Y. Liu, L. Qin, X. Chen, Z. Lin, and S. Liang, "Experimental and numerical studies on combustion character of solid-liquid rocket ramjet," in *Proc. 45th AIAA/ASME/SAE/ASEE Joint Propulsion Conf.*, Denver, CO, 2009.

[5] W. Miller, S. McClendon, and W. Burkes, "Design approaches for variable flow ducted rockets," in *Proc. AIAA/SAE/ASME 17th Joint Propulsion Conf.*, Springs, CO, 1981.

[6] C. Goldman and A. Gany, "Thrust modulation of ram-rockets by a vortex valve," in *Proc. AIAA/ASME/SAE/ASEE Joint Propulsion Conf. and Exhibit*, Lake Buena Vista, FL, 1996.
[7] A. Atwood, T. Boggs, T. P. P. O. Curran, and D. Hanson-Parr, "Burning rate of solid propellant ingredients, part 1: Pressure and initial temperature effects," *J. Propulsion Power*, vol. 15, no. 6, pp. 740–747, Nov.–Dec. 1999.
[8] J. Chang, B. Li, W. Bao, W. Niu, and D. Yu, "Thrust control system design of ducted rockets," *Acta Astronaut. (U.K.)*, vol. 69, no. 1, pp. 86–95, 2011.
[9] W. Bao, B. Li, J. Chang, W. Niu, and D. Yu, "Switching control of thrust regulation and inlet buzz protection for ducted rocket," *Acta Astronaut. (U.K.)*, vol. 67, no. 7, pp. 764–773, 2010.
[10] W. Bao, Y. Qi, and J. Chang, "Multi-objective regulating and protecting control for ducted rocket using a bumpless transfer scheme," *Proc. Inst. Mech. G, J. Aerosp. Eng.*, vol. 227, no. 2, pp. 311–325, 2012.
[11] Y. Qi, W. Bao, J. Zhao, and J. Chang, "Coordinated control for regulation/protection mode-switching of ducted rockets," *Acta Astronaut. (U.K.)*, vol. 98, pp. 138–146, May–June 2014.
[12] Y. Qi, W. Bao, J. Chang, and J. Cui, "Fast limit protection design: A terminal sliding mode control method," in *Proc. 33rd Chinese Control Conf.*, Nanjing, China, pp. 26–30, 2014.
[13] D. Thomaier, "Speed control of a missile with throttleable ducted rocket propulsion," in *Proc. Advances Air-Launched Weapon Guidance and Control,* 1987, p. 15.
[14] A. G. Sreeriatha and N. Bhardwaj, "Mach number control-ler for a flight vehicle with ramjet propulsion," in *Proc. AIAA/ASME/SAE/ASEE 35th Joint Propulsion Conf. and Exhibit*, Los Angeles, CA, 1999.
[15] P. Pinto and G. Kurth, "Robust propulsion control in all flight stages of a throtteable ducted rocket," in *Proc. AIAA/ASME/ASEE Joint Propulsion Conf. and Exhibit*, San Diego, CA, 2011, pp. 1–12.
[16] W. Bao, W. Niu, C. J. T, T. Cui, and D. Yu, "Control system design and experiment of needle-type gas regulating system for ducted rocket," *Proc. Inst. Mech. Eng. G, J. Aerosp. Eng.*, vol. 224, no. 5, pp. 563–573, 2010.
[17] W. Y. Niu, W. Bao, J. Chang, T. Cui, and D. R. Yu, "Control system design and experiment of needle-type gas regulating system for ducted rocket," *J. Aerosp. Eng.*, vol. 224, no. 5, pp. 563–573, 2010.
[18] C. Bauer, N. Hopfe, P. Caldas-Pinto, F. Davenne, and G. Kurth, "Advanced flight performance evaluation methods of supersonic air- breathing propulsion system by a highly integrated model based approach," in *Proc. RTO-MP-AVT-208*, 2012, pp. 1–14.
[19] A. Ilchmann, E. P. Ryan, and C. J. Sangwin, "Tracking with prescribed transient behaviour," *ESAIM Control Optim. Calculus Variations*, vol. 7, pp. 471–493, July 2002.
[20] H. Schuster, C. Westermaier, and D. Schroder, "Non-identifier-based adaptive control for a mechatronic system achieving stability and steady state accuracy," in *Proc. IEEE Int. Conf. Control Applications*, 2006, pp. 1819–1824.
[21] O. J. Smith, "A controller to overcome dead time," *ISA J.*, vol. 6, pp. 28–33, 1959.
[22] A. Z. Manitius and A. W. Olbrot, "Finite spectrum assignment problem for systems with delays," *IEEE Trans. Autom. Control*, vol. AC-24, no. 4, pp. 541–552, Aug. 1979.
[23] K. Ichikawa, "Frequency-domain pole assignment and exact model-matching for delay systems," *Int. J. Control*, vol. 41, no. 4, pp. 1015–1024, 1985.
[24] R. Ortega and R. Lozano, "Globally stable adaptive controller for systems with delay," *Int. J. Control*, vol. 47, no. 1, pp. 17–23, 1988.
[25] S.-I. Niculescu and A. M. Annaswamy, "An adaptive smith-controller for time-delay systems with relative degree $n^* \leq 2$," *Syst. Control Lett.*, vol. 49, no. 5, pp. 347–358, 2003.
[26] D. Bresch-Pietri and M. Krstic, "Adaptive trajectory tracking despite unknown input delay and plant parameters," *Automatica*, vol. 45, no. 9, pp. 2074–2081, Sept. 2009.
[27] N. Bekiaris-Liberis and M. Krstic, "Delay-adaptive feedback for linear feedforward systems," *System Control Lett.*, vol. 59, no. 5, pp. 277–283, May 2010.
[28] A. J. Calise and T. Yucelen, "Adaptive loop transfer recovery," *J. Guid. Control Dyn.*, vol. 35, no. 3, p. 807, 2012.
[29] M. Krstic, *Delay Compensation for Nonlinear, Adaptive, and PDE Systems*. Boston, MA: Birkhauser, 2009.
[30] M. Matsutani, A. M. Annaswamy, T. E. Gibson, and E. Lavretsky, "Trustable autonomous systems using adaptive control," in *Proc. Decision and Control and European Control Conf.*, 2011, pp. 6760–6764.
[31] B. C. Gruenwald, T. Yucelen, and J. A. Muse, "Model reference adaptive control in the presence of actuator dynamics with applications to the input time-delay problem," in *Proc. American Institute Aeronautics and Astronautics Guidance Navigation and Control Conf.*, 2017, p. 1491.
[32] K. Abidi, Y. Yildiz, and B. Korpe, "Explicit time-delay compensation in teleoperation: An adaptive control approach," *Int. J. Robust Nonlinear Control*, vol. 26, no. 15, pp. 3388–3403, Oct. 2016.
[33] Y. Yildiz, A. Annaswamy, D. Yanakiev, and I. Kolmanovsky, "Spark ignition engine idle speed control: An adaptive control approach," *IEEE Trans. Control Syst. Technol.*, vol. 19, no. 5, pp. 990–1002, 2011.
[34] Y. Yildiz, A. Annaswamy, D. Yanakiev, and I. Kolmanovsky, "Spark ignition engine fuel-to-air ratio control: An adaptive control approach," *Control Eng. Pract.*, vol. 18, no. 12, pp. 1369–1378, 2010.
[35] D. Bresch-Pietri and M. Krstic, "Delay-adaptive control for nonlinear systems," *IEEE Trans. Autom. Control*, vol. 59, no. 5, pp. 1203–1218, May 2014.
[36] M. Trnk, J. Murga, E. Miklovicov, and L. Farkas, "Adaptive control of time-delayed systems with application for control of glucose concentration in type 1 diabetic patients," in *Proc. Int. Federation Automatic Control Volumes*, Caen, France, 2013, vol. 46, pp. 452–457.
[37] J. P. Nelson and M. J. Balas, "Model reference adaptive control of spacecraft attitude for a PNP satellite with unknown time varying input/output delays," in *Proc. IEEE Int. Systems Conf.*, Vancouver, Canada, 2012.
[38] J. Haddad and B. Mirkin, "Adaptive perimeter traffic control of urban road networks based on MFD model with time delays," *Int. J. Robust Nonlinear Control*, vol. 26, pp. 1267–1285, Jan. 2016. doi: 10.1002/rnc.3502.
[39] Y. Yildiz, A. Annaswamy, I. Kolmanovsky, and D. Yanakiev, "Adaptive posicast controller for time-delay systems with relative degree $n^* \leq 2$," *Automatica*, vol. 46, no. 2, pp. 279–289, 2010.
[40] T.-G. Lee and U.-Y. Huh, "An error feedback model based adaptive controller for nonlinear systems," in *Proc. IEEE Int. Symp.* Industrial Electronics, Guimaraes, Portugal, 1997, pp. 1095–1100.
[41] T. Gibson, A. Annaswamy, and E. Lavretsky. (2012, Oct.) Adaptive systems with closed-loop reference models: Stability, robustness, and transient performance, arXiv Preprint, arXiv:1201.4897. [Online]. Available: http://arxiv.org/abs/1201.4897
[42] T. Gibson, A. Annaswamy, and E. Lavretsky, "Improved transient response in adaptive control using projection algorithms and closed loop reference models," in *Proc. American Institute Aeronautics and Astronautics Guidance Navigation and Control Conf.*, Minneapolis, MN, 2012.
[43] T. Gibson, A. Annaswamy, and E. Lavretsky, "On adaptive control with closed-loop reference models: Transients, oscillations, and peaking," *IEEE Access*, vol. 1, pp. 709–717, Sept. 2013.
[44] J. H. Lee, B. H. Park, and W. Yoon, "Parametric investigation of the pintle-perturbed conical nozzle flows," *Aerosp. Sci. Technol.*, vol. 26, no. 5, pp. 268–279, 2013.
[45] R. Deng, T. Setoguchi, and H. D. Kim, "Computational study on the thrust performance of a supersonic pintle nozzle," in *Proc. Int. Symp. Turbulence and Shear Flow Phenomena*, Melbourne, Australia, 2015.
[46] J. Heo, K. Jeong, and H.-G. Sung, "Numerical study of the dynamic characteristics of pintle nozzles for variable thrust," *J. Propulsion Power*, vol. 31, no. 1, pp. 230–237, 2015.
[47] H. Ko, J.-H. Lee, H.-B. Chang, and W.-S. Yoon, "Cold tests and the dynamic characteristics of the pintle type solid rocket motor," in *Proc. 49th AIAA/ASME/SAE/ASEE Joint Propulsion Conf.*, San Jose, CA, 2013.
[48] J. H. Lee, J. K. Kim, H. B. Jang, and J. Y. Oh, "Experimental and theoretical investigations of thrust variation with pintle positions using cold gas," in *Proc.44th AIAA/ASME/SAE/ASEE Joint Propulsion Conf. and Exhibit*, Hartford, CT, 2008.
[49] S. B. Verma and O. Haidn, "Cold gas testing of thrust-optimized parabolic nozzle in a high-altitude test facility," *J. Propulsion Power*, vol. 27, no. 6, pp. 1238–1246, Nov.–Dec. 2011.
[50] Z. W. Peterson, S. D. Eilers, and S. A. Whitmorey, "Closed-loop thrust and pressure profile throttling of a nitrous-oxide HTPB hybrid rocket motor," in *Proc. 48th AIAA/ASME/SAE/ASEE Joint Propulsion Conf. and Exhibit*, Atlanta, GA, 2012.
[51] K. S. Narendra and A. M. Annaswamy, *Stable Adaptive Systems*. New York: *Dover Publications*, 2005.
[52] E. Lavretsky and K. A. Wise, *Robust Adaptive Control*. London: Springer, 2013.
[53] Y. Yildiz, A. M. Annaswamy, D. Yanakiev, and I. Kolmanovsky, "Spark-ignition-engine idle speed control: An adaptive control approach," *IEEE Trans. Control Syst. Technol.*, vol. 19, no. 5, pp. 990–1002, Sept. 2011.
[54] T. E. Gibson, "Closed-loop reference model adaptive control: With application to very flexible aircraft," Ph.D. dissertation, Massachusetts Inst. Technol., 2014.